ADVANCING EARTH AND SPACE SCIENCES

JGR Atmospheres

RESEARCH ARTICLE
10.1029/2022JD037697

Flood Impacts on Net Ecosystem Exchange in the Midwestern and Southern United States in 2019

Nikolay V. Balashov[1,2], Lesley E. Ott[1], Brad Weir[1,3,4], Sourish Basu[1,2], Kenneth J. Davis[5,6], Natasha L. Miles[5], Anne M. Thompson[7,8], and Ryan M. Stauffer[7]

[1]NASA Global Modeling and Assimilation Office (GMAO), Goddard Space Flight Center, Greenbelt, MD, USA, [2]Earth System Science Interdisciplinary Center, University of Maryland, College Park, MD, USA, [3]Universities Space Research Association, Columbia, MD, USA, [4]Now at Morgan State University, Baltimore, MD, USA, [5]Department of Meteorology and Atmospheric Science, The Pennsylvania State University, University Park, PA, USA, [6]Earth and Environmental Systems Institute, The Pennsylvania State University, University Park, PA, USA, [7]Earth Sciences Division, NASA Goddard Space Flight Center, Greenbelt, MD, USA, [8]University of Maryland, Baltimore County, Baltimore, MD, USA

Key Points:

- A devastating flood occurred in 2019 over the Midwestern and Southern regions of the US significantly affecting ecosystem carbon cycling
- Net ecosystem exchange is examined in the flood-effected areas with NASA's GEOS modeling system from 2017 through 2019
- The 2019 floods caused a net reduction in Midwestern crop carbon uptake and smaller net increase in non-crop uptake in Southern states

Supporting Information:

Supporting Information may be found in the online version of this article.

Correspondence to:

N. V. Balashov,
nikolay.v.balashov@nasa.gov

Citation:

Balashov, N. V., Ott, L. E., Weir, B., Basu, S., Davis, K. J., Miles, N. L., et al. (2023). Flood impacts on net ecosystem exchange in the Midwestern and Southern United States in 2019. *Journal of Geophysical Research: Atmospheres*, *128*, e2022JD037697. https://doi.org/10.1029/2022JD037697

Received 19 AUG 2022
Accepted 28 AUG 2023
Corrected 26 OCT 2023

This article was corrected on 26 OCT 2023. See the end of the full text for details.

Abstract Climate extremes such as droughts, floods, heatwaves, frosts, and windstorms add considerable variability to the global year-to-year increase in atmospheric CO_2 through their influence on terrestrial ecosystems. While the impact of droughts on terrestrial ecosystems has received considerable attention, the response to flooding is not well understood. To improve upon this knowledge, the impact of the 2019 anomalously wet conditions over the Midwest and Southern US on CO_2 vegetation fluxes is examined in the context of 2017–2018 when such precipitation anomalies were not observed. CO_2 is simulated with NASA's Global Earth Observing System (GEOS) combined with the Low-order Flux Inversion, where fluxes of CO_2 are estimated using a suite of remote sensing measurements including greenness, night lights, and fire radiative power as well as with a bias correction based on insitu observations. Net ecosystem exchange CO_2 tracers are separated into the three regions covering the Midwest, South, and Eastern Texas and adjusted to match CO_2 observations from towers located in Iowa, Mississippi, and Texas. Results indicate that for the Midwestern region consisting primarily of corn and soybeans crops, flooding contributes to a 15%–25% reduction of annual net carbon uptake in 2019 in comparison to 2017 and 2018. These results are supported by independent reports of changes in agricultural activity. For the Southern region, comprised mainly of non-crop vegetation, annual net carbon uptake is enhanced in 2019 by about 10%–20% in comparison to 2017 and 2018. These outcomes show the heterogeneity in effects that excess wetness can bring to diverse ecosystems.

Plain Language Summary Carbon dioxide (CO_2) is the main driver of climate change whose atmospheric concentration is governed by a mix of human emissions and absorption by land and ocean sinks. Understanding how these sinks will respond to climate change in the future, including in response to increasingly frequent extreme events like floods, is critical in setting reliable emission reduction targets and improving Earth system models. Here, the devastating flood of 2019 that affected the Midwestern and Southern US is examined with respect to its effects on the ability of land ecosystems to absorb CO_2. The analysis is performed using NASA's GEOS model, which simulates CO_2 concentrations based on a simple land model that had previously been adjusted to match global background insitu observations. In this study, fluxes are adjusted using CO_2 observations from measurement towers in the U.S. Simulations covering the years of 2017–2019 are compared and indicate that parts of the affected region absorbed less CO_2 in 2019 than in previous years. The results demonstrate the effects of floods on the carbon cycle are complex and warrant further study, which is needed to understand how land ecosystems will respond to climate change in the future.

1. Introduction

Understanding the future evolution of the carbon cycle is crucial to improve climate change predictions (Frank et al., 2015). Studies show that climate extremes (i.e., extreme weather events) have a noticeable effect on terrestrial ecosystems influencing the cycling of carbon and thereby affecting global atmospheric CO_2 concentrations (Frank et al., 2015; Reichstein et al., 2013). These extremes are characterized by meteorological phenomena such as droughts, floods, heat waves, frosts, and windstorms (Reichstein et al., 2013). While general understanding regarding how these extremes affect the global carbon cycle exists, each case presents a unique challenge that may

deviate from expected behavior. To better understand the effects of climate extremes on carbon exchange between terrestrial ecosystem and atmosphere, detailed analysis of relevant case studies is required.

Droughts are common extreme weather events that impact terrestrial ecosystem carbon processes and are relatively well studied (van der Molen et al., 2011). In the time of drought, the ability of an ecosystem to consume CO_2 decreases (Frank et al., 2015; Schwalm et al., 2012). While the impact of droughts on terrestrial ecosystem has received considerable attention over the recent years, the response of an ecosystem to flooding events is intricate and ambiguous (Dalmagro et al., 2019; Dušek et al., 2009; Knapp et al., 2008; Miyata et al., 2000; Zaerr, 1983; Zona et al., 2012). As the climate changes, climate models predict an increase in precipitation for midlatitude regions, thereby increasing the likelihood of flooding events affecting these ecosystems (Knapp et al., 2008; Zhang & Villarini, 2021). Therefore, it is imperative to better understand how the potential increase in flooding events may affect future carbon budget.

The effects of flooding on carbon exchange in the terrestrial ecosystem depends on the type of vegetation affected. Wetlands tend toward storing less atmospheric carbon during flooding as photosynthesis weakens; however, annual Net Ecosystem Exchange (NEE) may not change much as ecosystem respiration (RE) also decreases (Han et al., 2015). Typically, during a growing season trees, shrubs, and grasses support net uptake of atmospheric CO_2 and continue to do so during moderate flooding, but it is not exactly clear how an increase in the magnitude of the flooding may alter this process (Bourtsoukidis et al., 2014; Detmers et al., 2015; Kramer et al., 2008). Ma et al. (2016) found that grasslands in Australia can even benefit from anomalously wet conditions and assimilate more carbon compared to normal soil moisture conditions. Croplands, however, are easily susceptible to waterlogging and tend to be a net source of atmospheric carbon when flooding occurs (Ahmed et al., 2013; Rosenzweig et al., 2002; Yildirim & Demir, 2022; Yin et al., 2020). Although the majority of CO_2 that is initially absorbed by croplands is eventually released back into the atmosphere, the cropland soils have the capacity to sequester atmospheric CO_2 and their ability to hold carbon is critically important for reducing global atmospheric CO_2 levels (Follett, 2001; Paustian et al., 2000; Zomer et al., 2017). Also, extreme precipitation events may cause topsoil erosion leading to additional carbon emissions into the atmosphere (Dinsmore et al., 2013; Hilton et al., 2008; Lal, 2019). To further the knowledge of the effects of flooding on ecosystem carbon fluxes, the spring/early summer Midwestern and central Southern US anomalously wet conditions of 2019 are investigated.

Heavy precipitation in the spring/early summer of 2019 resulted in widespread flooding of the Upper Mississippi River Basin and the surrounding regions causing damages in the range of 2–3 billion US dollars (Neri et al., 2020; Price & Berkowitz, 2020; Reed et al., 2020). The focus of this study is on the Midwest (M) and the South (S and T, Figure 1), where anomalously wet conditions affected areas with different types of vegetation. Stream gauges levels along with variety of other data and survey reports indicate that the M region experienced periods of major flooding while the regions S and T were only partially affected (Section S1 in Supporting Information S1). In the Midwest vegetation primarily consists of croplands such as maize (corn) and soybeans, while in the South there are mainly forests transitioning to prairies in Eastern Texas (Figure 1). The primary aim of this study is to investigate the impact of the 2019 anomalously wet conditions on the NEE with simulations from NASA's Goddard Earth Observing System (GEOS) Low-order Flux Inversion (LoFI) model in the affected regions, in contrast to the years 2017 and 2018 which experienced comparatively lower anomalous precipitation levels, and to assess results in the context of the regional GEOS LoFI NEE climatology from the period 2000–2016.

Previously, Yin et al. (2020) showed the ability to quantify Midwest atmospheric CO_2 and Midwest croplands gross primary production (GPP) anomalies during the abovementioned 2019 flood using XCO_2 measurements from the Orbiting Carbon Observatory 2 (OCO-2) and solar-induced chlorophyll fluorescence (SIF) derived from the TROPOspheric Monitoring Instrument (TROPOMI). Comparing 2019 to 2018, their results suggest a reduction in the Midwest cropland GPP of −0.21 Pg C in June and July and partial recovery of 0.14 Pg C in August and September. Additionally, they noted a flood-forced 3-week delay in the planting date of crops across much of the area. Turner et al. (2021) also used TROPOMI SIF to study the impacts of the 2019 flood on CONUS vegetation arriving at similar conclusions as Yin et al. (2020) with 2018 as a reference year.

The present study builds upon Yin et al. (2020) and Turner et al. (2021) by analyzing optimized GEOS LoFI NEE of the flood-affected region over the period 2017–2019 using insitu tower data and extending the comparison to GEOS LoFI 2000–2016 regional NEE climatology. The focus is on better understanding of the 2019 precipitation event and its impact on the affected ecosystems from the perspective of the atmospheric carbon monitoring system. Specifically, the study looks at monthly and annual regional optimized NEE budgets for years 2017–2019

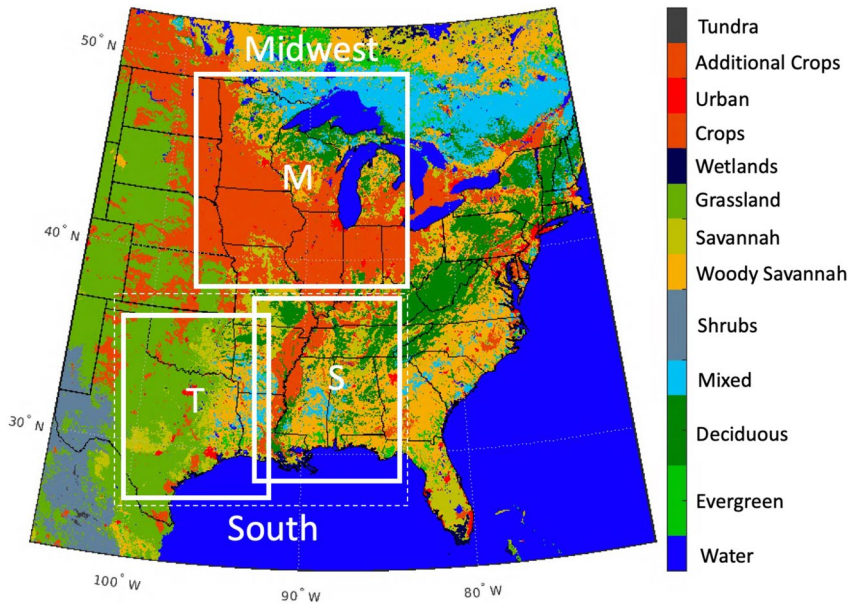

Figure 1. Land cover map of the Eastern Conterminous United States (CONUS) derived from Moderate Resolution Imaging Spectroradiometer (MODIS). White rectangles indicate regions affected by the anomalous precipitation and are the focus of this study. Capital letter M indicates the Midwest region, while capital letters S (South) and T (Texas) represent regions of the South (for more details see Data and Methods section).

comparing them to the GEOS LoFI 2000–2016 NEE budget climatology. The key scientific inquiry at hand is determining the extent to which the 2019 late spring/early summer flood in the Midwest and parts of the South has impacted the annual NEE budget, and whether this impact is significant enough to be observable with the tools employed. Additionally, the performance of the NASA near real time carbon modeling tool, GEOS LoFI, is assessed and implications for carbon monitoring are discussed.

2. Data and Methods

2.1. MERRA-2

To map out regions of the flooding in 2019, precipitation, root zone soil wetness, and 2-m temperature data from the Modern-Era Retrospective analysis for Research and Applications, Version 2 (MERRA-2) are used (Gelaro et al., 2017). Bias corrected MERRA-2 precipitation (mm) comprised of background data products [such as Goddard Earth Observing System Model, version 5 (GEOS-5) or Forward Processing system for Instrument Teams (FP-IT)] and observations [i.e., Global Precipitation Climatology Project (GPCP)] is utilized (Reichle, Draper, et al., 2017; Reichle, Liu, et al., 2017). Root zone soil wetness is described by the ground wetness variable for the 0–100 cm layer of soil. The variable is dimensionless in units of relative saturation ranging from 0 to 1, where value of 1 indicates completely saturated soil. Root zone soil wetness, precipitation, and 2-m temperature May–August 2017–2019 anomalies with respect to May–August 1981–2010 climatology are calculated over the region of interest.

2.2. Crop Data

Since croplands contribute significantly to the carbon cycle of the M region, 2017–2019 United States Department of Agriculture (USDA) crop planting data are analyzed for corn (maize) and soybeans—the two most common crops in the US Midwest. In this study, three attributes, which are crop planting progress, acres planted, and grain yield of corn and soybeans from years 2017–2019 are compared. The following states are analyzed here: Illinois, Indiana, Iowa, Kansas, Michigan, Minnesota, Missouri, Nebraska, Ohio, South Dakota, and Wisconsin. The data is taken from National Agriculture Statistics Service provided by USDA (https://quickstats.nass.usda.gov/).

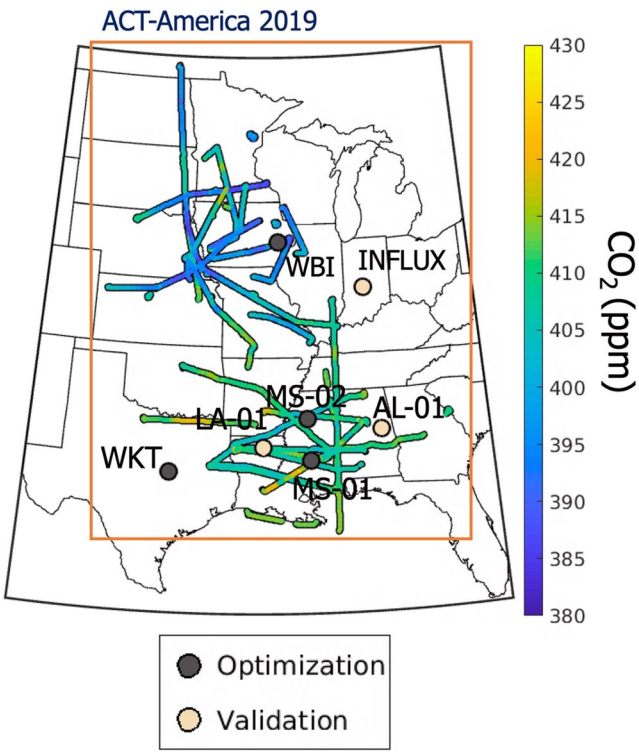

Figure 2. CO_2 observations that are used for the GEOS model optimization and validation. Aircraft transect CO_2 mole fractions are shown inside the ABL and are used for validation. Towers are labeled by circles.

2.3. CO_2 Data

2.3.1. Optimization Data

The optimization of the GEOS model (described later in Section 2.6) takes place in two different areas, the Midwest (M) and the South (broken down into two regions: S and T, Figure 1). The process of optimization consists of adjusting GEOS NEE CO_2 tracers from the 3 regions (M, S, and T) over the 3 years (2017–2019) in an attempt to match 5-day running mean of daily observations [averaged over the afternoon hours of 1500–1700 local standard time (LST)] from insitu CO_2 towers located in the regions of interest: West Branch, Iowa (WBI) in M, Magee, Mississippi (MS-01) in S, Grenada, Mississippi (MS-02) in S, and Moody, Texas (WKT) in T (see Figure 2).

The WBI tower is in the agricultural ecosystem (corn belt) of eastern Iowa and is part of the National Oceanic and Atmospheric Administration (NOAA) Earth System Research Laboratories/Global Monitoring Laboratory (ESRL/GML) tall tower network that is tasked with the goal of long-term carbon-cycle gas monitoring in the atmospheric boundary layer (ABL) of continental areas (Andrews et al., 2014; Schuldt et al., 2021). The location of the tower is ideal for CO_2 monitoring pertinent to the Midwestern croplands and hence is used here to analyze the effects of the 2019 flooding.

MS-01 and MS-02 towers are in Mississippi and were instrumented initially for the Gulf Coast Intensive, designed to characterize CO_2 in the southeastern region of the US and maintained through 2019 as part of the airborne Atmospheric Carbon and Transport-America (ACT-America) project (Miles et al., 2018). The MS towers did not measure CO_2 simultaneously; therefore, to represent CO_2 of the S region, MS-01 is used for 2017 and MS-02 is used for 2018–2019. These towers are well suited for this study as the state of Mississippi did see significant wet anomalies in 2019 but avoided major flooding that occurred upstream of the state.

Finally, WKT represents the T region of the South. Like WBI, the tower is part of the NOAA ESRL/GML tall tower network (Andrews et al., 2014). The location of the tower is optimal for capturing CO_2 variability in eastern Texas and western Louisiana, where the flooding of 2019 was also partially present.

2.3.2. Validation Data

Validation process with tower-based and airborne measurements is aimed at determining how well the towers used for the optimization act as a proxy for the regions of interest. The M region is validated with the Indianapolis Flux Experiment (INFLUX) background tower 1 that is located on the southwestern part of Indianapolis, the direction least influenced by the CO_2 emissions from the city (Davis et al., 2017). As in Iowa (where WBI is located), vegetation in Indiana mainly consists of crops, making it a good choice for the validation of the model optimizations at WBI. However, INFLUX tower 1 is immediately surrounded by forests, in contrast to WBI. The S and T regions are validated using towers in Millerville, Alabam (AL-01) and Monroe, Louisiana (LA-01). To be consistent with the optimization, 5-day running mean of daily observations (averaged over the afternoon hours of 1500–1700 LST) is utilized.

The 2019 ACT-America campaign is also used for validation. ACT-America is an airborne NASA Earth Venture mission dedicated to improving the accuracy, precision, and resolution of atmospheric inverse estimates of CO_2 and CH_4 sources and sinks on a regional scale (Davis et al., 2021). The mission conducted five seasonal campaigns (including two summer campaigns) over the 2016–2019 period. For each campaign two aircraft (C-130 and B-200) were used to survey three different regions in the United States: The South, the Midwest, and the Mid-Atlantic. Data from the 2019 campaign covering the South and the Midwest is used, which occurred in June and July of 2019. Most of the flights took place in the period of 1100–1700 LST. For validation purposes the boundary layer [~330 m above ground level (AGL)] CO_2 was averaged for each of the selected flight days.

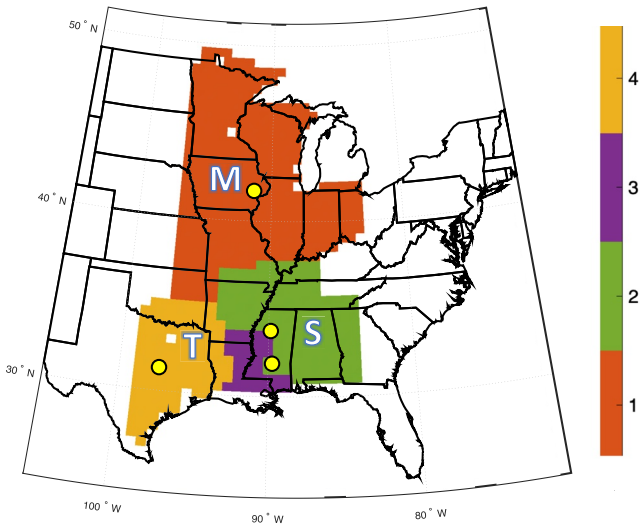

Figure 3. Masks for the optimization based on the backward HYSPLIT trajectories, where red region 1 influences WBI tower in Iowa and is labeled as M NEE CO_2 tracer, the green region 2 influences MS-01 and MS-02 towers in Mississippi and is labeled as S NEE CO_2 tracer, the purple region 3 influences both MS and WKT towers (part of both S and T NEE CO_2 tracers), and finally the yellow region 4 influences WKT tower in Texas and is labeled as T NEE CO_2 tracer. Yellow circles indicate towers used for optimization.

2.4. GEOS Model Configuration Including LoFI Flux Package

NASA GEOS general circulation model, constrained by MERRA-2 meteorology fields, with resolution of 0.5° by 0.625° and 72 vertical layers (Molod et al., 2015) is utilized to simulate CO_2 over the region of interest from 14th January to 14th December for the years 2017–2019 (Weir et al., 2021). It includes the Low-order Flux Inversion (LoFI) package, which contains a compilation of carbon fluxes driven by remote-sensing land surface data (Ott et al., 2015; Weir et al., 2021) and a bias correction process designed to reproduce CO_2 mole fractions observed at NOAA's in situ network. There are five components to the mentioned LoFI flux package: NEE, biomass burning, fossil fuel combustion, ocean exchange, and an empirical land sink (bias correction of the fluxes).

NEE is computed using the Carnegie-Ames-Stanford Approach—Global Fire Emissions Dataset version 3 (CASA-GFED 3; Randerson et al., 1996; Van der Werf et al., 2010) that estimates carbon fluxes using satellite-derived vegetation products and MERRA-2 meteorology. Biomass burning CO_2 emissions are derived with the Quick Fire Emissions Dataset (QFED; Koster et al., 2015), which is constructed using MODIS fire radiative power (FRP) estimates in near real-time. Fossil fuel combustion is provided by the Open-source Data Inventory for Anthropogenic CO_2 (ODIAC; Oda & Maksyutov, 2015; Oda et al., 2018) that is based on disaggregated country-level fossil fuel CO_2 emission inventories using a global power plant database and satellite observations of nighttime lights. Ocean exchange of CO_2 is estimated using the differences between the partial pressure of CO_2 in seawater (pCO^{sw}_2) derived from the Takahashi et al. (2009) climatology and the partial pressure in the atmosphere (pCO^{atm}_2) taken from the NOAA marine boundary layer (MBL) reference (Dlugokencky & Tans, 2016; Masarie & Tans, 1995). An empirical land sink is applied as a bias correction to the collection of fluxes to constrain the modeled atmospheric CO_2 growth with the observed growth rates derived from the NOAA MBL reference (Weir et al., 2021). The empirical sink matches the global total fluxes for a year to a specified atmospheric growth rate of CO_2 by reducing heterotrophic respiration during months when there is an increase in the 2-m air temperature, which is used as an approximate indicator of soil temperature, compared to the previous month.

In addition to using LoFI as a driver of GEOS CO_2 simulation, it is also used to compute 2000–2016 monthly and annual NEE climatology that could be used as a supplemental metric for comparison to initial and optimized 2017–2019 NEE. Monthly 2000–2016 NEE climatology is computed by averaging the sum of 3-hourly NEE values for each month (except January and December) over the 17 years and annual climatology is computed by summing all 3-hourly NEE values for each year and then finding an average of these 17 sums. Due to the way the model is ran, for January 3-hourly values from the dates of 18th through 31st are summed and for December 3-hourly values from the dates of 1st through 14th are summed. Furthermore, monthly spatial NEE 2017–2019 anomalies of regions M, S, and T with respect to spatial monthly 2000–2016 NEE climatology are computed (Section S6 in Supporting Information S1).

2.5. Definition of Tagged Tracer Regions

Before the optimization an area that influences towers is designated using NOAA's Hybrid Single-Particle Lagrangian Integrated Trajectory (HYSPLIT) model backward trajectories (Stein et al., 2015). The trajectories are released backwards for every 6 hr for May through September of 2019 at the three optimization towers WBI, MS-02 (it is assumed MS-02 is representative of MS-01), and WKT from the level of the corresponding sensor (121–379 m AGL) using the North American Regional Reanalysis (NARR) meteorology. The approximate area influencing each tower combined with the MODIS Land Cover Climate Modeling Grid Product (MCD12C1) allow for the generation of CO_2 mole fraction tracer masks applied to tag regional NEE within GEOS that can be then used in the optimization (Figure 3). MCD12C1 is the reprojection of the tiled MODIS Land Cover Type Product (MCD12Q1) with the sub-pixel proportions of each land cover class in each 0.05° pixel and the aggregated quality assessment information from the International Geosphere-Biosphere Program (IGBP) scheme

(Sulla-Menashe & Friedl, 2018). MCD12C1 is used to generate the appropriate masks of vegetation areas of interest while removing any urban and coastal environments.

2.6. Optimization Approach

To quantify the effects of 2019 flooding on regional vegetation, NEE is compared to the years 2017 and 2018. Though NEE is available from the LoFI flux package, it is possible that these fluxes are inaccurate because of the use of a highly simplified diagnostic vegetation model. To provide a better estimate, the NEE component of the LoFI collection, representative of the vegetation fluxes of a given area, is adjusted to minimize the model-observation CO_2 mole fraction difference. The optimization is independently performed for the three different regions of M, S, and T (Figure 3), where each region is characterized by its individual NEE CO_2 tracer based on the selected insitu towers.

The observed CO_2 mole fraction can be expressed in the following way:

$$CO2_{obs} = CO2_{model} + \Delta CO2, \tag{1}$$

where $CO2_{model}$ represents CO_2 from GEOS and $\Delta CO2$ is the mole fraction of CO_2 that needs to be added to the modeled mole fraction to arrive at the observed value. The $CO2_{model}$ term can be expanded as

$$CO2_{model} = CO2_{ini} + CO2_{ocn} + CO2_{FF} + CO2_{fire} + CO2_{NEE}, \tag{2}$$

where $CO2_{ini}$ is an initial condition that consists of all the accumulated CO_2 at a particular model grid cell in the model prior to January 14th of a given year (either 2017, 2018, or 2019) and the rest of the right-hand terms are additions from ocean (OCN), fossil fuels (FF), fire, and NEE. In the current work it is hypothesized that NEE term is the most uncertain and that the $\Delta CO2$ term in Equation 1 is mainly driven by the $CO2_{NEE}$ term. Therefore, it is the only term adjusted to bring the modeled CO_2 closer to the observed CO_2. The $CO2_{NEE}$ tracer is tracked by the model from the selected regions and the rest of the globe as shown in Figure 3 and can be expressed as

$$CO2_{NEE} = CO2^{M}_{NEE} + CO2^{S}_{NEE} + CO2^{T}_{NEE} + CO2^{global}_{NEE}, \tag{3}$$

with the right hand terms representing regional and the rest of the globe NEE CO_2 tracers. Only the regional tracers are adjusted in this study.

The optimization is performed at each of the three towers (M, S, and T) by solving for the minimum value of the cost function (Rodgers, 2000):

$$J(a) = \frac{1}{2}\left[\left(\hat{y} + \alpha CO2^{region}_{NEE}\right) - y\right] R^{-1} \left[\left(\hat{y} + \alpha CO2^{region}_{NEE}\right) - y\right]^T + \frac{1}{2}\alpha B^{-1}\alpha^T, \tag{4}$$

where α is a scaling factor by which NEE needs to be changed, $\hat{y}$ is modeled 5-day running mean of daily afternoon (1500–1700 LST) averages of CO_2, y is observed 5-day running mean of daily afternoon (1500–1700 LST) averages of CO_2, B is the scaling factor error covariance term, and R is the observation-model error covariance matrix. B can be a matrix if more than one tracer is optimized, but in the current case of optimizing just one tracer, B becomes equivalent to $\sigma^2_{\alpha_p} = 0.5$, which determines by how much the scaling factor α can be adjusted from the initial scaling factor $\alpha_p = 0$. The value of 0.5 is empirically derived and in this case is just large enough to allow for physically reasonable NEE variation. R matrix represents combined observation-model error as well as the covariances among the days in each segment. The adjustment is performed on a total of 22 segments consisting of 15 daily y and $\hat{y}$ values to smooth out NEE daily variability over the time of about 2 weeks (Chevallier et al., 2012; Friend et al., 2007). Square matrix R is generated by first calculating observation-model daily error terms ε with the expression (Heald et al., 2004):

$$\varepsilon = y - \hat{y} - \overline{y - \hat{y}}. \tag{5}$$

Then ε terms are divided into 22 segments consisting of consecutive 15 daily values from the total of m daily values (in this case total is 330 days comprising most of the year). Variance is calculated for each segment as follows,

$$\sigma^2_i = \frac{\left(\sum_{i=1}^{15} \varepsilon_i\right)^2}{15 - 1}. \tag{6}$$

This variance is unique to each segment and repeated for every day inside of an individual segment. Afterward, the variance is converted to standard deviation σ (by taking a square root) and the initial version of R is

$$R = \begin{bmatrix} \sigma_1^2 & r_{12}\sigma_1\sigma_2 & \dots & r_{1m}\sigma_1\sigma_m \\ r_{21}\sigma_2\sigma_1 & \sigma_2^2 & \dots & r_{2m}\sigma_2\sigma_m \\ \vdots & \vdots & \ddots & \vdots \\ r_{m1}\sigma_m\sigma_1 & r_{m2}\sigma_m\sigma_2 & \dots & \sigma_m^2 \end{bmatrix}, \tag{7}$$

where the covariance terms representing propagation of error in time are modified by coefficient

$$r_{ij} = e^{-|i-j|/d}, \tag{8}$$

with d being a time scale. After the completion of the initial optimization, R is adjusted using reduced χ^2 statistic when initial term α becomes available for every segment with 22 being the total number of optimized segments,

$$\chi^2 = \frac{1}{22}\left[\left(\hat{y} + \alpha CO2_{NEE}^{region}\right) - y\right] R^{-1} \left[\left(\hat{y} + \alpha CO2_{NEE}^{region}\right) - y\right]^T. \tag{9}$$

For each segment, σ is modified until reduced χ^2 approximately approaches a value of 1 and final value of α is determined.

The error covariance of α is estimated with

$$\hat{R} = \left[\left(CO2_{NEE}^{region}\right)^T R^{-1} CO2_{NEE}^{region} + B^{-1}\right]^{-1}. \tag{10}$$

Once α is estimated, it is used to construct an optimized time series of CO_2 mole fractions along with its variation based on the estimated vector $\hat{R}$ (which provides 22 values of $\sigma_{optimized}$) by randomly drawing 1,000 times from the normal distribution in the following fashion,

$$\alpha^* = \alpha + Normal(0, \sigma_{optimized}). \tag{11}$$

Then α and α^* are used to generate optimized CO_2 time series with the corresponding noise:

$$CO2_{optimized} = CO2_{model} + \alpha CO2_{NEE}^{region}, \tag{12}$$

$$CO2^*_{optimized} = CO2_{model} + \alpha^* CO2_{NEE}^{region}. \tag{13}$$

Afterward, the adjusted NEE is estimated by summing the LoFI NEE $\left(NEE_{model}^{region}\right)$ over all the pixels of each region (M, S, and T) in 15-day increments and then using

$$NEE_{optimized}^{region} = NEE_{model}^{region} + \alpha NEE_{model}^{region}. \tag{14}$$

The optimized NEE for each month is computed by summing the appropriate derived increments. For January, dates of 18th through 31st are used for the summation and for December dates of 1st through 14th are summed. The total annual NEE is found by adding all the 22 segments of each year. The uncertainties of 15-day increments are represented by the variance values from the $\hat{R}$ and uncertainties of the monthly and annual NEE are found by summing corresponding variances.

3. Results and Discussion

3.1. Relevant Meteorology and Its Effects on Crops

Figure 4 shows precipitation, root zone soil wetness, and 2-m temperature anomalies for the eastern and central US over the years of 2017–2019 during the period of May-August when most of the 2019 flooding and its effects occurred. Comparing May–August precipitation totals over the years 2017–2019 indicate that 2019 (Figure 4c) saw noticeable wet anomalies in the central US including the Midwest and the South with the

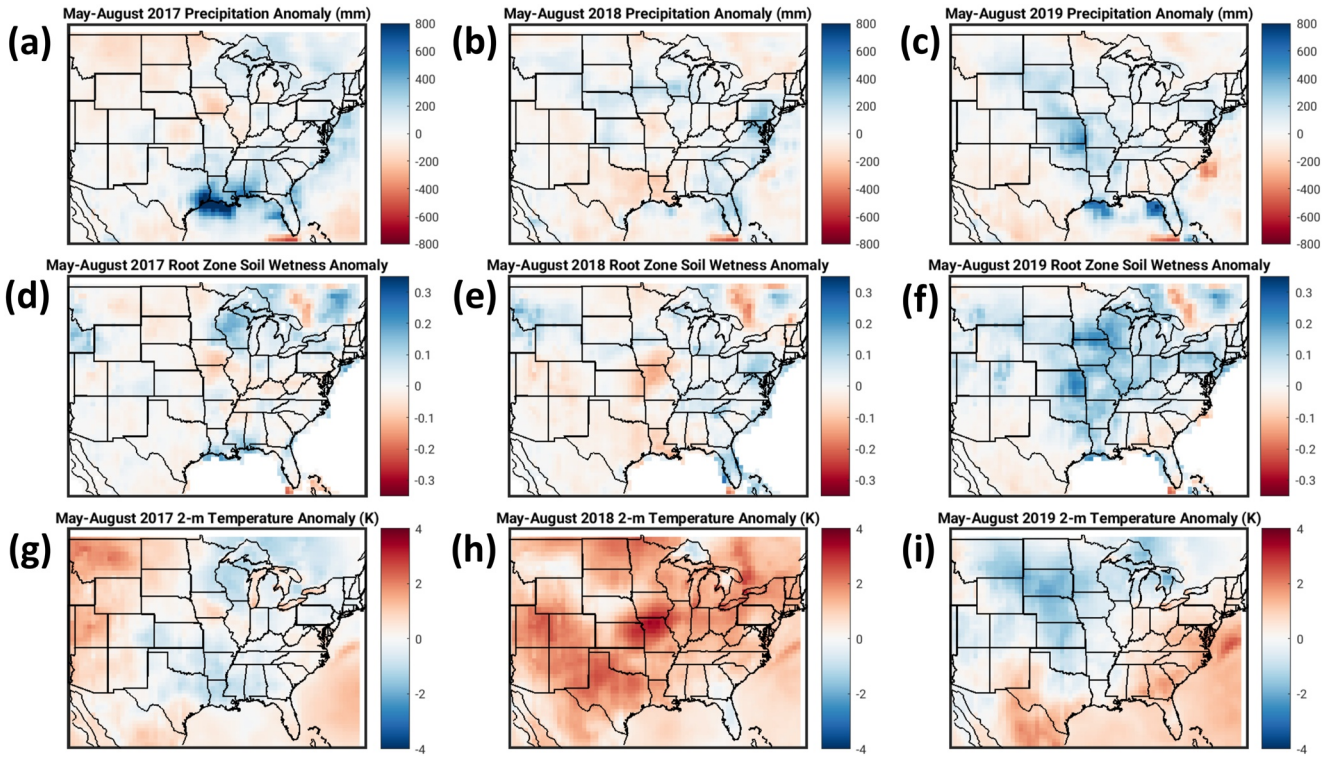

Figure 4. Precipitation, root zone soil wetness, and 2-m temperature August-May anomalies with respect to 1981–2010 climatology from MERRA-2 (Gelaro et al., 2017) in the eastern and central US for years 2017–2019, where panels (a), (b), and (c) correspond to precipitation anomalies over 2017–2019, panels (d), (e), and (f) correspond to root zone soil wetness over 2017–2019, and panels (g), (h), and (i) correspond to 2-m temperature anomalies over 2017–2019.

Midwest experiencing much of the flooding and the South only being partially affected (more information about the flood is in Section S1 in Supporting Information S1). The same regions in 2017 and 2018 (Figures 4a and 4b) generally saw negative anomalies except for coastal regions of southeastern Texas, southern Louisiana, southern Mississippi, and southern Alabama in 2017, when extremely wet conditions occurred. More evidence of the 2019 flood can be gleaned from the widespread root zone soil wetness positive anomalies in May-August of 2019 (Figure 4f) in comparison to May-August of 2017 and 2018 (Figures 4d and 4e), although some slightly positive anomalies can be seen in Wisconsin and coastal gulf states in 2017. Surface (2-m) temperature anomalies over May–August in 2019 are mostly below normal in the Midwest and close to normal values in the eastern regions, while in May–August of 2018 whole shown area except for Florida is well-above average, and 2017 in general is unremarkable.

The immediate effects of 2019 flooding on the two major US crops are evident from Figure 5, where in Figures 5a and 5b planned planting of corn and soybeans is delayed by almost a month. The delay is likely caused by the severe waterlogging that occurred in early May not allowing farmers to proceed with the planned crop planting timetables. Figures 5c and 5d indicate that the total planted annual acres of corn and soy are about 3%–15% lower in 2019 than in years 2017 and 2018. Figures 5e and 5f show both corn and soy yields are lower in 2019 in comparison to 2017 and 2018.

These results are also partially supported by Figure S3 in Supporting Information S1 exhibiting Fraction of Photosynthetically Active Radiation (FPAR) anomalies for years 2017–2019. FPAR indicates plant's ability to incorporate solar radiation to promote its growth (more details are included in Section S2 in Supporting Information S1; Los et al., 2000). The figure shows noticeable negative FPAR anomalies in parts of the Midwest over 2019 suggesting that the flood was significant enough to affect plant function and to cause pronounced reduction of crop yields in the Midwest compared to years 2017 and 2018. This may imply that the amount of carbon assimilated by the crops is also lower in 2019 than in the two prior years. This hypothesis as well as the possible opposite effects of the anomalously wet conditions on the non-crop vegetation (positive FPAR anomalies in the S and T regions) is addressed in the next section.

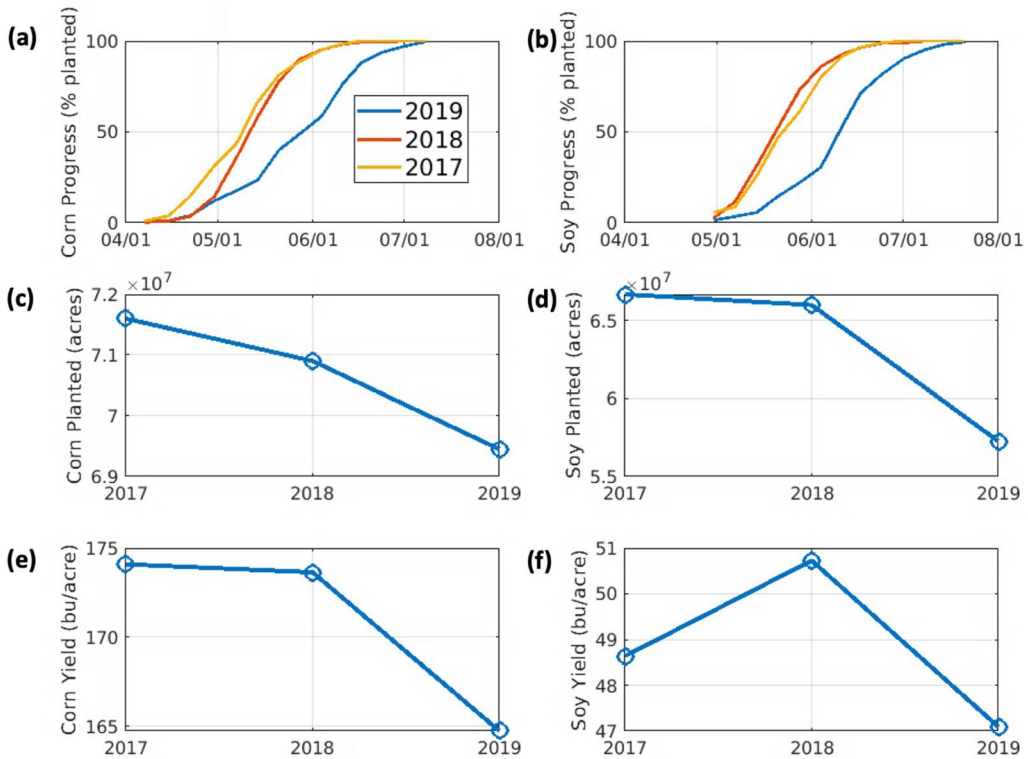

Figure 5. Corn and soybean statistics in the Midwestern states (listed in Section 2.2) showing progress (percent planted), acres planted, and yield for the years 2017–2019, where (a), (c), and (e) indicate the mentioned statistics for corn and (b), (d), and (f) for soy (https://quickstats.nass.usda.gov/).

3.2. NEE Optimization in the Midwest and the South

In Figure 6, the results of the optimization process are presented by comparing the optimized GEOS CO_2 time series with the original non-optimized GEOS CO_2 time series and the tower observations. Uncertainty of the optimization is denoted by gray lines representing one sigma variation. The time series are 5-day running daily means plotted as the days of year at the regions M, S, and T over the years 2017–2019. The adjustments made because of the optimization process (explained in Section 2.6) are illustrated in Figure 7, which shows nine time series of the resultant scaling factors for GEOS NEE CO_2 tracer mole fractions reflecting the time series shown in Figure 6. The scaling factors in Figure 7 are plotted in a such way that positive values indicate a need to increase uptake in the model, while negative values indicate a need to decrease uptake in the model. Scaling factor uncertainty of one sigma is shown by black lines.

Beginning with the analysis of CO_2 cycle in the M region (Figures 6a–6c), growing seasons differ for each of the years with 2017 having the earliest drawdown start day on about 100th day of the year as evident from Figure 6a. The model picks up this feature in 2017 generally well, but with incorrect magnitude. The years 2018 and 2019 exhibit slightly later drawdown start days with 2019 experiencing the beginning of the net uptake earlier than 2018 by about 10–20 days. For both years the model erroneously predicts the start of growing season around the day 100. The peak period of net uptake lasts about 20–30 days longer in 2017 compared to 2018, and only a few days longer compared to 2019. Overall, the model performs adequately in replicating the shape of the drawdown cycle; however, during the peak net uptake period, it appears to exhibit a deficiency in the necessary uptake.

Upon further examination of the model's performance in the M region, it is discovered that during the 3-year period, scaling factors shown in Figures 7a–7c demonstrate comparable characteristics, although with variations in magnitude. The principal trends of GEOS LoFI model biases in region M are identified as insufficient uptake during the first 50 days, excessive uptake between days 100 and 170, inadequate uptake from around day 170 to approximately day 230, elevated uptake from roughly day 250 to day 300, and insufficient uptake during the remainder of the year. The year 2018 necessitates the most significant optimization adjustments, particularly within the period spanning from day 100 to approximately day 220.

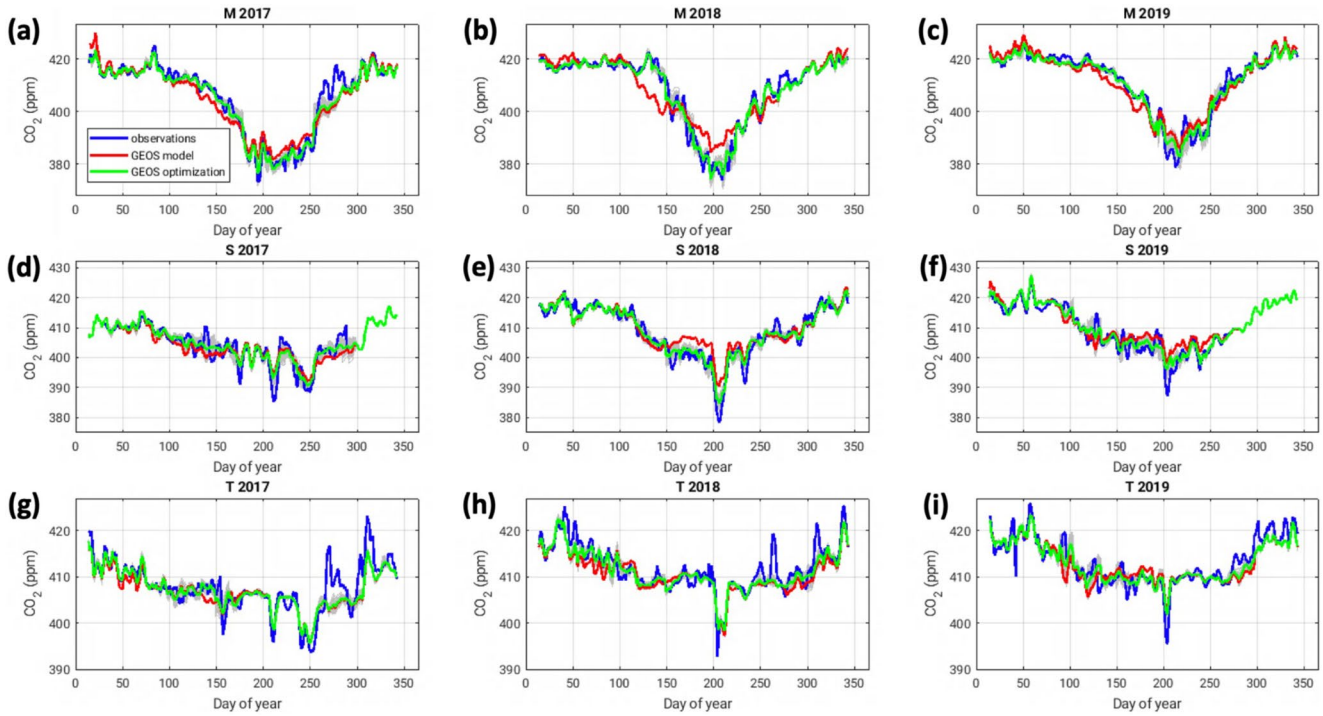

Figure 6. CO_2 insitu observations versus GEOS model along with its optimization for towers WBI, MS (1 and 2), and WKT located in M, S, and T regions, where (a) WBI in 2017, (b) WBI in 2018, (c) WBI in 2019, (d) MS-01 in 2017, (e) MS-02 in 2018, (d) MS-02 in 2019, (g) WKT in 2017, (h) WKT in 2018, (i) WKT in 2019.

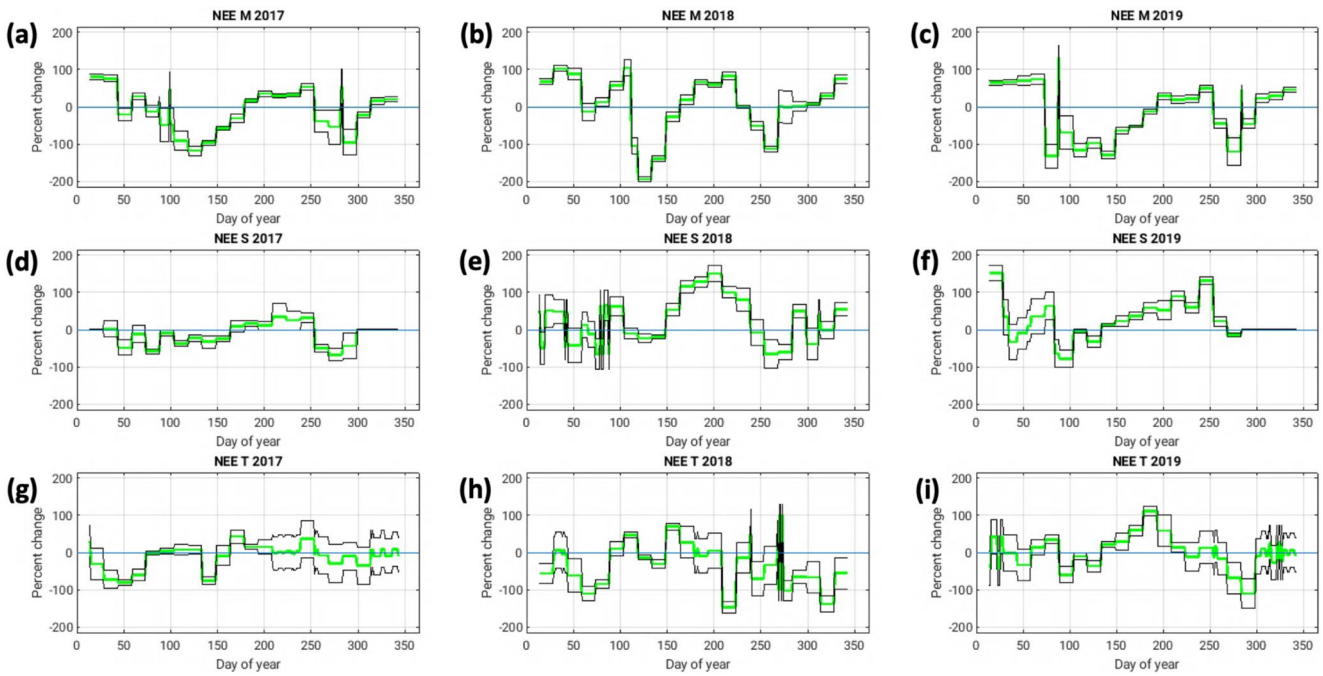

Figure 7. Regional scaling factors (shown in green) in percentages of GEOS NEE CO_2 tracer mole fractions as a function of day of year derived at towers WBI, MS (1 and 2), and WKT located in M, S, and T regions, where (a) WBI in 2017, (b) WBI in 2018, (c) WBI in 2019, (d) MS-01 in 2017, (e) MS-02 in 2018, (d) MS-02 in 2019, (g) WKT in 2017, (h) WKT in 2018, (i) WKT in 2019. Black lines indicate one sigma interval of an overall uncertainty of an estimated scaling factor. The scaling factors are plotted in such a way as to indicate a decrease in carbon uptake when the scaling factor is negative and to indicate an increase in carbon uptake when the scaling factor is positive.

Possible explanations for some of the observed variations in drawdown cycle in the M region can be found in Figure 4. From a meteorological perspective, there are no remarkable anomalies observed in the Midwest region during 2017, while the years 2018 and 2019 exhibit anomalous levels of heat and precipitation, respectively. During the peak of growing season between May and August, Figure 4h reveals widespread positively anomalous 2-m temperatures encompassing the Midwest region in 2018. Also Figure 4e hints at some deficit in root zone soil wetness in some of the central states. These meteorological parameters indicate that spring and summer of 2018 experienced partial drought conditions, which led to a slight setback in corn progress (Figure 5a) delaying drawdown cycle. The year 2019 witnessed extreme flooding because of the above-normal precipitation illustrated in Figure 4c, and substantially increased root zone soil wetness as demonstrated in Figure 4f. These anomalously wet conditions impeded the growth of corn and soybean, as indicated in Figures 5a and 5b, consequently reducing carbon uptake.

Moving on to the S region (Figures 6d–6f), where the model generally tracks accurately tower observations except for a period in 2018 where it is too high. The growing season is much less defined in the S region than in the region M making it difficult to state exactly how it differs among the shown years. The drawdown begins earlier in the S region than in the M region by about 20–30 days. Additionally, the S region CO_2 time series exhibit an interesting feature in the form of noticeable jaggedness, which reflects variations in air masses. During summer, air moving from the north tends to be depleted in CO_2 as it passes over the widespread crop areas, resulting in dips in the time series (Figure S4 in Supporting Information S1). Conversely, air moving from the south tends to be enriched in CO_2 as it accumulates over the Gulf of Mexico, leading to spikes in the time series. In winter, CO_2 tends to pile up along a frontal boundary introducing spikes in CO_2 tower observations over the southern areas (Figures S5 in Supporting Information S1). Such spikes are also produced by spring frontal intrusions as higher-CO_2 air is brought to the South (where a growing season has already started) from the Midwest where the switch from efflux to uptake did not yet occur (Figure S6 in Supporting Information S1).

The scaling factors derived from the optimization for the S region shown in Figures 7d–7f share a few important similarities although also contain differences. All 3 years indicate a need for more uptake in the GEOS LoFI from about day 150 to about day 250. The time series markedly differ in magnitude of the scaling factors with 2017 showing the least amount of variation and 2018 with the most dramatic bias peaking at about 150%.

Meteorologically, the S region is slightly less affected by the temperature anomalies in 2018 and the root zone soil wetness anomalies in 2019; however, the mentioned features are still found in Figures 4h and 4f. Also, a large amount of coastal precipitation in 2017, evident from Figure 4a, makes year 2017 potentially atypical. It is difficult to make any conclusions about how the weather specifically affected vegetation carbon uptake in the S region over the years 2017–2019, but a little more analysis on this is presented in Section 3.4.

The T region is characterized by mostly consistent CO_2 time series with a slight hint of growing season beginning to occur early in a year, interspersed with occasional sharp drops and spikes (Figures 6g–6i), similar to what is observed in the S region. The NEE tracer derived from GEOS LoFI does not exhibit large values in the T region and therefore does not allow for much optimization. The model generally does a decent job predicting CO_2, but it consistently fails at identifying peaks of CO_2 suggesting challenges associated with carbon arriving from other areas.

In the T region, the scaling factors tend to be noisy, varying up and down, except for a period in 2019 from day 150 to day 200 where it is positive suggesting the need for more net carbon uptake in GEOS LoFI. The overall oscillatory nature of the scaling factor in the T region reflects the savanna/grasslands vegetation of the T region corresponding to the smaller values of NEE tracer that are hard to adjust effectively in comparison to the M and S regions.

3.3. Optimization Validation

In this study, the validation is meant to gauge the tower representativeness of each respective region by evaluating determined adjustments of the GEOS simulation using independent-from-optimization observations. The scaling factors derived at the optimization sites in all the three regions are combined and used to adjust CO_2 values at every validation site. The optimization described in the previous section is validated with three towers INFLUX, LA-01, and AL-01 and with data from the 2019 airborne ACT-America campaign. INFLUX tower results are demonstrated in Figures 8a–8c, where 5-day running daily averages of the observed, modeled, and

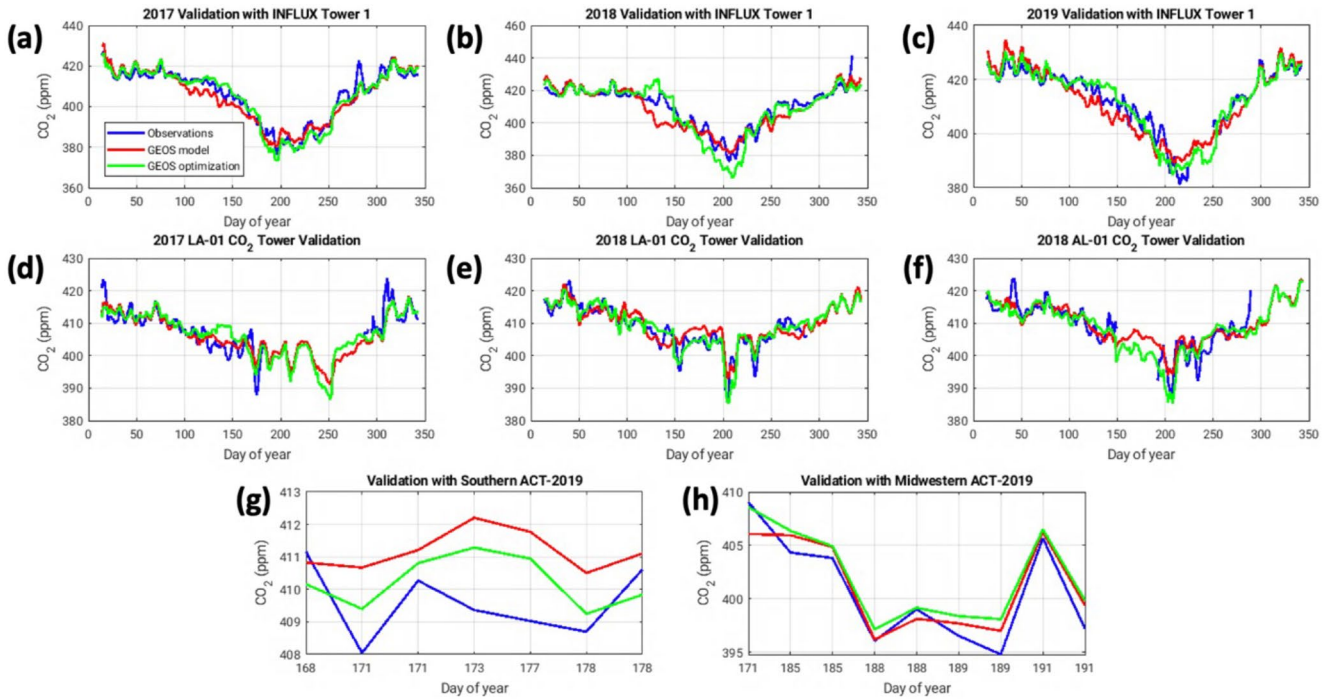

Figure 8. Validation of the optimization using various datasets throughout the years of interest, where the INFLUX tower 1 is shown in (a–c) for years 2017–2019, LA-01 tower is shown in (d–e) for years 2017–2018, AL-01 tower is shown in (f) for year 2018, Southern ACT-2019 daily averaged flights are shown in (g), and Midwestern ACT-2019 daily averaged flights are shown in (h).

model-adjusted CO_2 are plotted over a year. Comparing Figures 6a–6c and Figures 8a–8c indicates that the GEOS model bias is generally similar for both WBI and INFLUX towers although with different magnitudes—too much uptake in the first part of the growing season (days 100–160) and too little uptake at the heart of the drawdown (days 170–230). This result is reasonable as Indiana, like Iowa, is mainly an agriculture state (Figure 1). Therefore, the NEE optimization corrections (shown in green) adjust the model in the right direction. However, it is likely that the different vegetation in the proximity of INFLUX tower 1 (forests) and a somewhat different transport influence area affect the local CO_2 mole fractions.

Next, validation performed at LA-01 tower in years 2017 and 2018 is illustrated in Figures 8d and 8e. Validation at this tower serves to verify optimizations in both regions S and T. For the most part validation time series tend to line up well with observations demonstrating that MS-1, MS-2, and WKT towers are well representative of the S and T regions. The near-perfect alignment of optimized and observed values during days 150–200, as illustrated in Figure 8e is particularly impressive. Unfortunately, a significant portion of the observed data is missing in 2017. Also, it is possible to see that the correction of days 136–150 for 2017 (Figure 8d) is inconsistent with the Louisiana data. This discrepancy may imply that although the T and S regions share similarities they are not identical.

The only data that is available from the AL-01 tower is for 2018 and at that it is incomplete. The AL-01 tower can partially validate the S region optimization. Figure 8f shows that in the days 120–150 optimization is not helpful, but later in the period (starting at about day 210) some improvement can be noted confirming higher carbon uptake. In this regard 2018 LA-01 and AL-01 towers are consistent and support the evidence of too little uptake in the GEOS LoFI system at the peak of growing season.

Finally, airborne ACT-America 2019 campaign is used to validate the optimizations. ACT-America focused on all the regions of interest, first in the S and T regions during the second half of June (days 168–178) and then in the M region during the first part of July (days 185–191). Figure 8g compares airborne daily CO_2 averages to corresponding original and adjusted model values. Noticeable improvement can be seen in the adjusted model, signaling that the S and T regions likely did experience higher carbon uptake than the original GEOS calculation showed. Regarding ACT-America flights in the M region denoted in Figure 8h, the original and adjusted

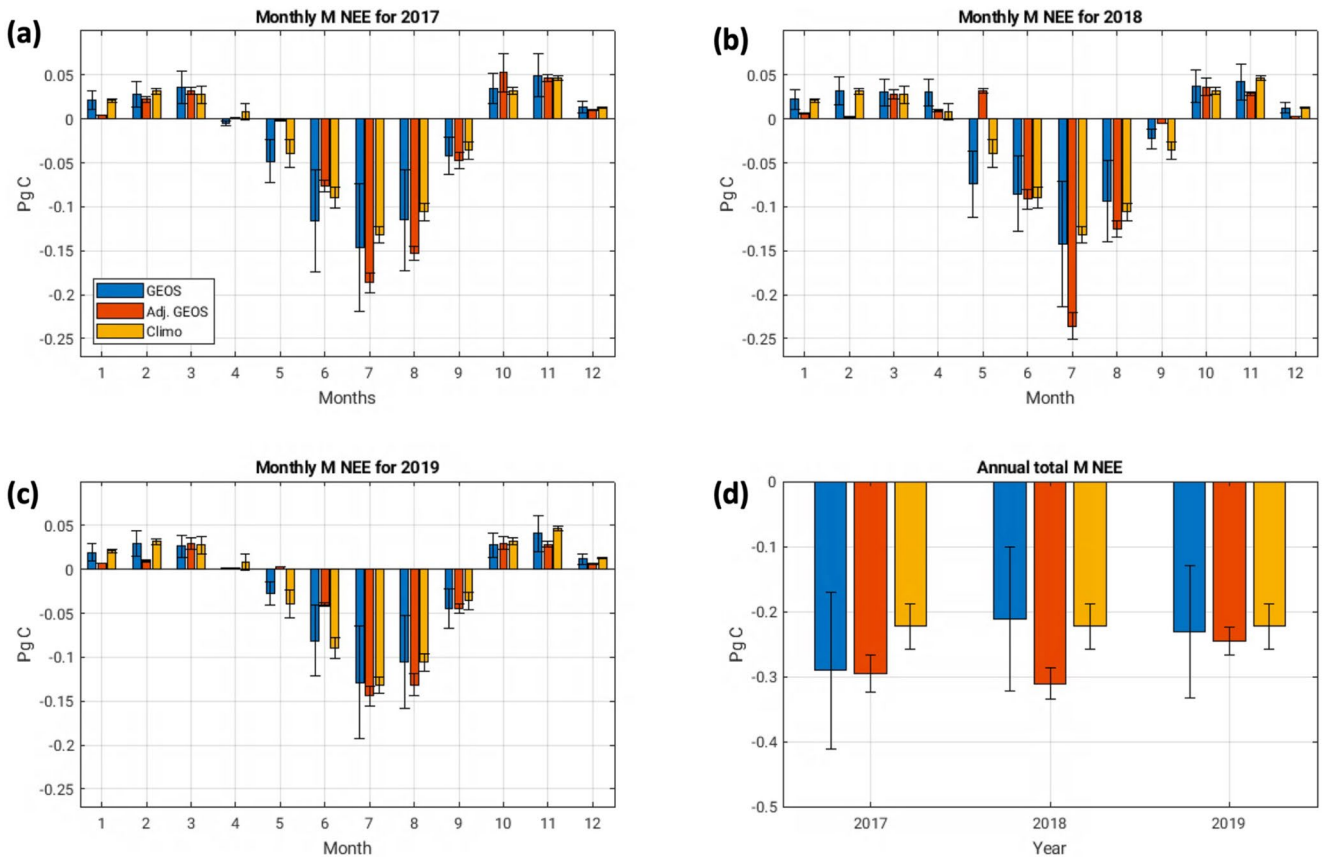

Figure 9. Original, adjusted, and climatological (2000–2016) GEOS NEE (in Pg of carbon) in the M region, where (a–c) panels show monthly flux for years 2017–2019 and (d) summarizes annual NEE flux for years 2017–2019. The uncertainty is one sigma.

models do not differ by much and generally closely resemble the airborne measurements. This is not surprising as Figure 7c suggests that in early July of 2019 (days 185–191) the model accurately estimated CO_2 mole fractions not requiring substantial adjustment.

Overall, the process of validating the optimizations showed that the derived scaling factors from the towers can be extended to the regions of interest albeit at times with a considerable error, which is difficult to quantify precisely. Established GEOS biases based on the WBI tower in the M region are partially observed at INFLUX tower 1. Regional ACT-America 2019 flights in the M region also indicate that the optimizations are reasonable. With regards to the S and T regions, towers LA-01 and AL-01 in 2018 and corresponding ACT-America 2019 flights show improved agreements with adjusted model fields. On the other hand, the LA-01 tower in 2017 does not suggest much improvement; however, this is a limited fragment of the overall validation dataset. Additionally, Figures S7 and S8 in Supporting Information S1 demonstrate a reverse process (Section S4 in Supporting Information S1), where validation sites are used to solve for the regions M, S, and T providing consistent results to the ones obtained in the current section.

3.4. Regional Annual NEE Variability

Once the optimization and validation procedures are accomplished it is possible to adjust GEOS NEE over all the regions and compare the outcomes among the years 2017–2019 as well as 2000–2016 LoFI climatology. Figure 9 presents a comparison of the monthly and annual original, adjusted, and climatological GEOS NEE for the M region, spanning the years 2017–2019. Figure 9a reflects Figure 6a, where 2017 begins to exhibit growing season sometime in April-May as optimized NEE is hovering around 0 Pg C. The growing season ends in October when net carbon source becomes apparent. Year 2018, as described in Section 3.2 (Figure 6b), displays a notably later inception to a growing season. Optimized NEE implies that net uptake begins sometime in June and ends in

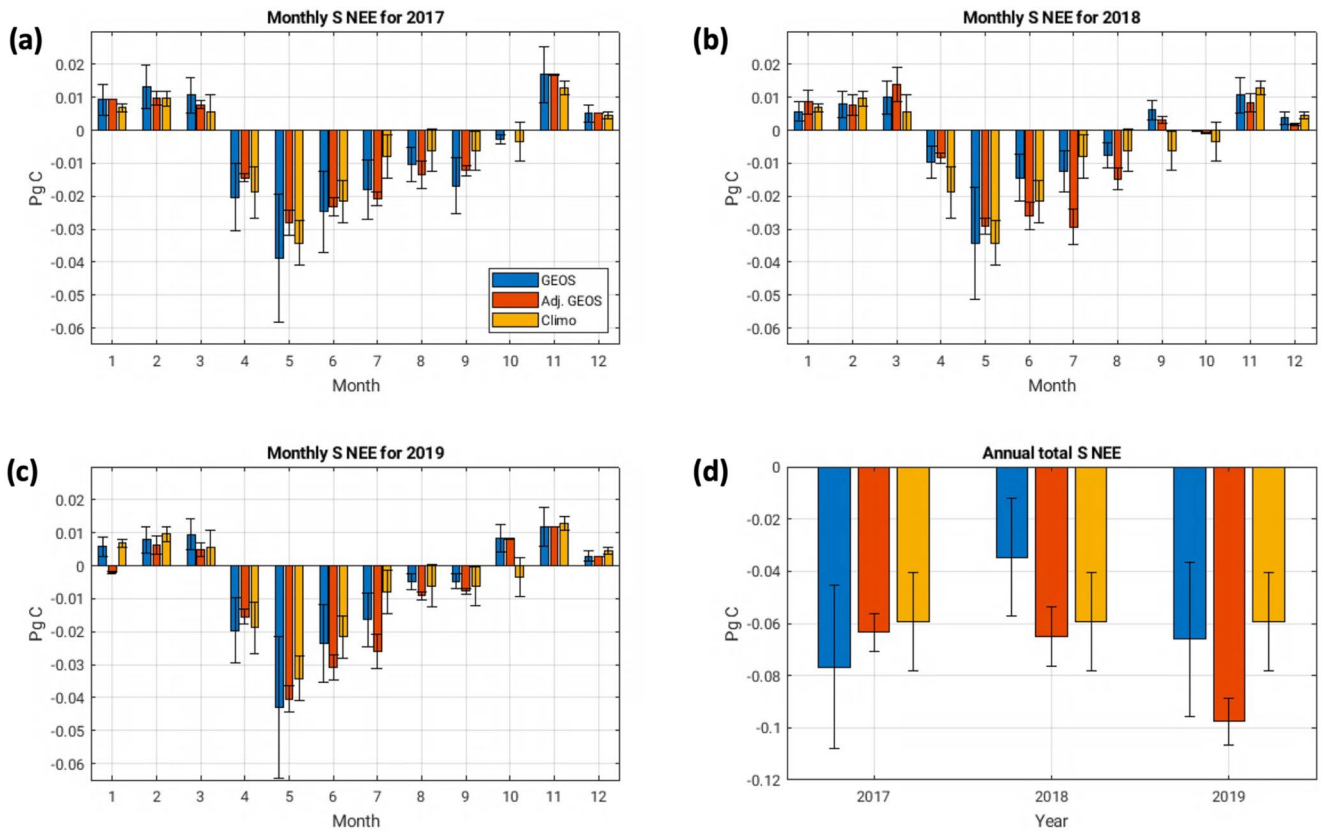

Figure 10. Original, adjusted, and climatological (2000–2016) GEOS NEE (in Pg of carbon) in the S region, where (a–c) panels show monthly flux for years 2017–2019 and (d) summarizes annual NEE flux for years 2017–2019. The uncertainty is one sigma.

October (Figure 9b). The delay of the growing season in 2018 is likely a result of the drought conditions (Haigh et al., 2022). Another interesting feature that could be spotted in 2018 is a drastic net uptake in July (Figure 9b), which can be explained by the fact that most of the crops in 2018 experienced an earlier than average blooming stage leading to a higher than usual net uptake in July but lower than usual net uptake in September. Although in the analysis of the optimized time series it appeared that 2019 had a delayed start to a growing season, Figure 9c seems to suggest that in terms of carbon uptake 2019 behaves similarly to 2017 in April–May despite experiencing the flood. It is only later in the growing season that 2017 is able to assimilate more carbon than the growing season of 2019 implying that if 2017 can be considered a normal year the impact of flooding on NEE was not instantaneous but delayed. However, determining whether 2017 qualifies as a typical year is not a simple matter (Section S6 in Supporting Information S1). As pointed out in Section 3.2, optimized NEE for all the 3 years conveys that non-optimized GEOS has not enough uptake in July and August.

An assessment of adjusted NEE yearly totals for the M region (Figure 9d) shows that 2019 has the least negative NEE compared to 2017 and 2018 supporting the assertion that the 2019 flood did reduce annual carbon uptake in the M region; however, the primary reduction in net uptake mainly occurred in June and July of 2019. The climatological LoFI NEE is close to the 2019 value indicating that the effect of this flooding on annual carbon budget may not be as unusual. It is important to note that the GEOS LoFI climatology is likely biased as it is based on the CASA model product that is known to underestimate carbon uptake over the US Midwestern croplands (Y. Zhou et al., 2020).

The overall growing season magnitude of negative NEE in the S region (Figures 10a–10c) is approximately four times lower than that of the M region. It is hypothesized here that this difference between M and S regions can be explained by the switch of vegetation from mostly crops to mixed forests and savannas (Figure 1). Crops such as corn and soybean that are abundant in the M region exhibit more efficient GPP with relatively less attendant RE than many other plant types (Guanter et al., 2014). Comparing GPP and RE outputs from GEOS

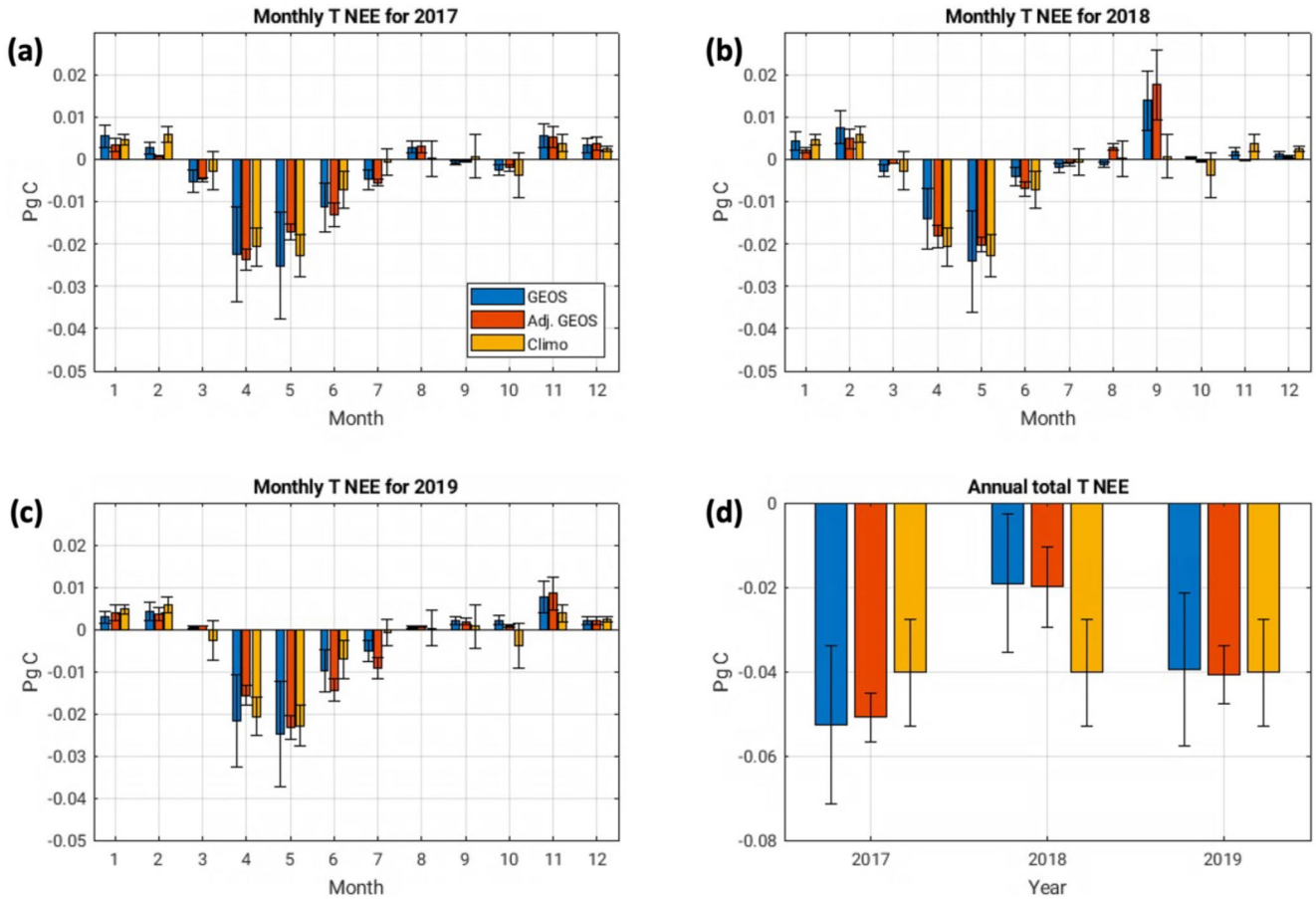

Figure 11. Original, adjusted, and climatological (2000–2016) GEOS NEE (in Pg of carbon) in the T region, where (a–c) panels show monthly flux for years 2017–2019 and (d) summarizes annual NEE flux for years 2017–2019. The uncertainty is one sigma.

LoFI between regions M and S in 2019 leads to similar conclusions (Figure S9 in Supporting Information S1). According to the examined 3 years and climatology the growing season in the S region appears to be from April to September-October. In 2017 the optimization does not significantly alter GEOS model fluxes, while noticeable changes are observed in 2018 and 2019. In years 2018 and 2019 the optimization implies that carbon uptake in the S region should be noticeably higher than what the original GEOS simulation indicates. That is especially true of 2018, where the annual uptake is increased by about 50% after the adjustment. Out of all the examined years, 2019 reveals the highest annual carbon uptake in the S region as evident from Figure 10d. This may indicate that the above-average rainfall of 2019 (Figure 4c) along with near or slightly above normal 2-m temperatures (Figure 4f) enhanced the regional plant growth, which is reflected by the higher than typical CO_2 drawdown. Climatological values of NEE tend to lack uptake from mid to late summer in comparison to 2017–2019 optimized values (Figures 10a–10c) implying potential systematic bias in GEOS LoFI.

The T region can be characterized by an even smaller NEE annual variability in comparison to the M and S regions reflecting the local vegetation consisting of grasslands and savannas (Figure 1). Figures 11a–11c imply shifted growing seasons from those in the regions M and S lasting from about March to early August. Although GEOS LoFI is generally in agreement with the optimization, it tends to show a net uptake that is too high during April and May. An interesting feature can be noted in Figure 11b, where September of 2018 exhibits relatively high net source of carbon in both GEOS LoFI and optimization. This could be potentially explained by the anomalously wet September that occurred that year in the region (National Centers for Environmental Information, 2018). Figure S10 in Supporting Information S1 indicates that RE rate surpassed GPP rate during September 2018 in the T region, which suggests that extreme precipitation significantly contributed to the net source of atmospheric carbon. In Figure 11d, 2018 has the least negative NEE likely attributable to the unseasonably warm conditions during the summer (Figure 4h) and extreme flooding in early fall. On the other hand, 2019 looks like a completely

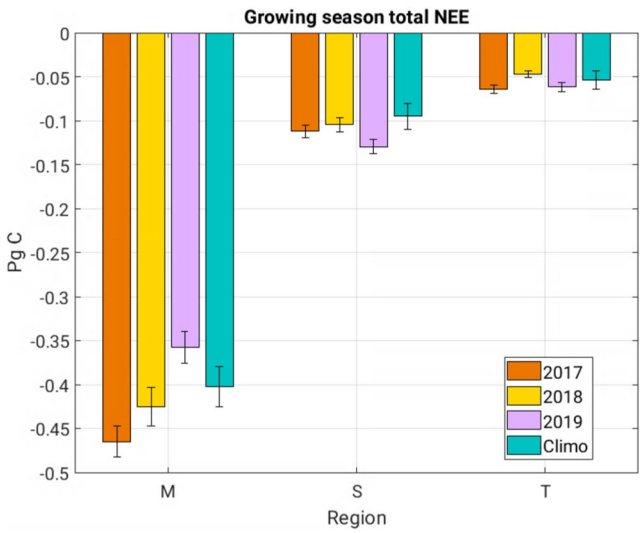

Figure 12. Optimized total growing season NEE for years 2017–2019 and corresponding LoFI 2000–2016 climatology as a function of a region. Growing seasons are defined as follows: May-September for the M region, April-September for the S region, and March-July for the T region. The uncertainty is one sigma.

normal year for the T region with annual carbon budget being near identical to the 2000–2016 regional climatology. Indeed, Figures 4c and 4f show that root zone soil wetness and precipitation fields are near normal in Texas for May-August period in 2019.

As an additional exploration, Section S6 in Supporting Information S1 examines spatial anomalies of NEE, GPP, and RE from the GEOS LoFI model (Figures S11, S12, and S13 in Supporting Information S1) and contrasts them against adjusted spatial NEE anomalies (Figure S14 in Supporting Information S1). All of the calculated anomalies are based on the LoFI 2000–2016 climatology and therefore should be treated with caution as the climatology itself is likely biased. This is supported by the optimization results shown in Figures 9–11. The bias is also evident in Figure S14 in Supporting Information S1 where generally for all the years it can be observed that May and June tend to have too much carbon uptake while July and August too little [with the exception of July 2019 (Figure S11c in Supporting Information S1), which is being affected by the flood]. Such consistent anomalies make it difficult to separate actual anomalies from the GEOS LoFI biases, but it could be concluded with a high measure of confidence that GEOS LoFI overpredicts carbon uptake in the first part of the growing season and underpredicts carbon uptake in the second half of the growing season. Interestingly, it is difficult to point out which NEE component is responsible for such a bias at any given situation as Figures S12 and S13 in Supporting Information S1 do not suggest consistent variations between GPP and RE indicating the complexity of the issue.

3.5. Effects of 2019 Flooding on NEE

After examining the annual variability of NEE at the M, S, and T regions for both 2017–2019 and the 2000–2016 LoFI climatology, it is now possible to contextualize the effects of the 2019 flooding on NEE within a broader perspective. The most significant impacts on NEE are apparent in the M and S regions, where the annual NEE budgets for 2019 stand out in contrast to years 2017–2018. In the M region, annual net carbon uptake is less than in years 2017–2018, but it is within the range of LoFI climatology value implying that the estimated NEE is not necessarily an extreme anomaly. For the S region, 2019 annual NEE is more negative than that in previous 2 years and LoFI climatology, which can be mainly attributable to the enhanced net uptake in May of 2019 (Figure 10c) when the precipitation event had the most influence.

These identified features in the M and S regions could be inspected further by looking at NEE budgets specifically for growing seasons. For the purpose of this study growing seasons are defined as a string of months with consistent negative NEE based upon Figures 9–11. As such the following timeframes are identified: May–September for the M region, April–September for the S region, and March–July for the T region. Figure 12 compares optimized NEE summed over a region for the years 2017–2019. The result is similar to what was previously discussed with year 2019 in the M and S regions exhibiting decreased and increased net uptakes respectively. In Figure 12 the impacts on NEE appear more pronounced as only growing seasons are considered, which were affected by the extreme precipitation more directly. Another important note to be made here is that regional drought in 2018 did not affect the M region NEE as markedly as the flood of 2019. Relatively small carbon flux variation over the T region suggests that the corresponding vegetation of grasslands and savannas is less affected by the wet conditions. Adding up all the surveyed information in this work it can be concluded that the flooding of 2019 did affect NEE significantly in the M and S regions and more so during the growing season when the consequences of the flood were most pronounced.

4. Conclusions

Generally prolonged excessive water conditions will negatively influence a plant system causing anoxia (W. Zhou et al., 2020); however, the effects of flooding on an ecosystem are not straightforward and largely depend on a

particular vegetation type and degree of waterlogging (Detmers et al., 2015; Sun et al., 2022). Wet conditions can result in an increase of carbon net uptake, but too much wetness may lead to a net carbon release because in these conditions both productivity and respiration tend to decrease, and the overall NEE balance will be contingent on specific environmental conditions (Ahlström et al., 2015; Bloch & Bhattacharjee, 2020). The current study affirms the mentioned assertions and implies that crops such as corn and soybeans seem to be more susceptible to waterlogging than non-crop vegetation such as savannas, forests, and grasslands. This is expressed in the reduced carbon uptake in the first part of the growing season over the Midwestern region of the US (mainly crops) and overall increased carbon uptake in the Southern region of the US (mainly non-crop) during the flood of 2019 when compared to 2017 and 2018. The change in 2019 annual NEE in the Midwest with respect to 2017 and 2018 of about 0.07 Pg C nearly equaled to the total magnitude of NEE in the regions S and T in 2019 when it was at the highest value among the examined years (−0.1 Pg C). For the perspective, an annual average NEE over the years 2010–2019 in North America is about −0.5 Pg C (Jiang et al., 2022). In addition, significant slowdown of the crop planting progress occurred in the early growing season of 2019 as most of the corn and soybeans in the US are in the Midwest. Flooding impacts in managed ecosystems dominated the net effect for the 2019 event. As humans are considering a variety of strategies to tackle climate change, sustainable crop management practice can accelerate carbon input into the soil (Meena et al., 2020). The exact effect of flooding on such practices is unclear but the delay in planting of crops explored in the current work raises questions that could influence future carbon balance and should be considered in strategies to reduce net emissions.

The impact of flooding on NEE and atmospheric CO_2 is readily observed by satellites (Yin et al., 2020) and a variety of in situ observational approaches (this study). Like Yin et al. (2020), for the Midwestern region this study finds a decrease in net carbon uptake over June and July of 2019 of about 0.06–1.2 Pg C [roughly 12%–24% of an average annual carbon net uptake in North America (Jiang et al., 2022)] when compared to both 2017 and 2018 and an increase in net carbon uptake in August and September of near 0.05 Pg C (roughly 10% of an average annual carbon net uptake in North America) when compared to 2018 [Note that Yin et al. (2020) estimated Gross Primary Production (GPP), which does not account for RE, while this study estimated NEE]. However, the results from the current study suggest that comparing 2019 to 2018 may not be optimal as 2018 may not be representative of an average growing season carbon activity (Jiang et al., 2022). For instance, assessment of 2019 NEE values with 2017 NEE values does not seem to show a "recovery" in August-September time frame as stated in Yin et al. (2020) and Turner et al. (2021) implying that additional inquiries are required into the detailed effects of flooding on the carbon uptake. Atmospheric CO_2 observations can play an important role in helping to monitor the impact of agricultural systems but require sustained planning and coordination (e.g., the discontinuity in towers made this study more difficult).

Finally, the assessment of the GEOS LoFI model shows that the model can simulate large-scale variations of CO_2 with notable skill in the Midwest and parts of the South, but some biases are evident. For instance, more uptake is required in the second part of the summer across all the examined regions, while uptake generally tends to be too high in May over the Midwest. These biases are consistent with Y. Zhou et al. (2020) study, which evaluated CASA against flux towers and other ecosystem models. Given that the GEOS LoFI is based on CASA such result is not surprising. Additionally, the model struggled to replicate CO_2 during passages of frontal systems that appear as spikes and dips in time series, specifically in the South. This could be attributable to the fact that LoFI is a monthly product downscaled to provide daily fluxes, which lacks the needed resolution to accurately represent day-to-day variations in CO_2 (Weir et al., 2021).

Overall, the low latency flux estimation approach from LoFI is credible in discerning flooding and non-flooding events, which demonstrates the maturity of modeling tools that can be applied to carbon monitoring at the current stage. Further investigations in this direction are imperative as only a sparse amount of literature is available regarding carbon exchange between an ecosystem and the atmosphere in a variety of water-excess conditions.

Data Availability Statement

CO_2 data from MS-01, MS-02, AL-01, and LA-01 towers are available at https://sites.psu.edu/gulfcoast/data/; also see Miles et al. (2018). WBI and WKT tower data are available here: https://gml.noaa.gov/ccgg/obspack/index.html. All of the crop data used in this article can be found at https://quickstats.nass.usda.gov/. ACT-America airborne data are located at https://actamerica.ornl.gov/airborne_data.shtml. SCOAPE data are stored at https://www-air.larc.nasa.gov/missions/scoape/index.html. MERRA-2 data used for GEOS forcing, temperature,

precipitation, and root zone soil wetness analyses are available at https://gmao.gsfc.nasa.gov/reanalysis/MERRA-2/. Source code for the NASA GEOS model is available under the NASA Open-Source Agreement at http://open-source.gsfc.nasa.gov/projects/GEOS-5. The NEE fluxes used in GEOS are based on the CASA-GFED dataset located at GES DISC (https://disc.gsfc.nasa.gov/datasets/GEOS_CASAGFED_3H_NEE_3/summary). All of the simulations used in this work are available upon request. More extensive descriptions of tower and airborne data can be found in Wei et al. (2021) and Masarie et al. (2014).

Acknowledgments
This work is supported by NASA's Carbon Monitoring System (NNH16DA001N-CMS 16-CMS16-0054, NNH20DA001N-CMS 20-CMS20-0011), NASA Postdoctoral Program (NPP), and a contract appointment with Earth System Science Interdisciplinary Center (ESSIC) at University of Maryland (UMD). We thank NASA Goddard Space Flight Center (GSFC) facility for providing us with the tools needed to perform the simulations used in this work. Also, we wish to thank ACT-America and Feasibility Study on Using Satellite-based Data for Offshore Air Quality Monitoring (SCOAPE) teams for helping us with specific questions pertinent to the data considered in the current study. Much gratitude to the reviewers who provided in-depth reviews that tremendously helped to improve the article.

References

Ahlström, A., Raupach, M. R., Schurgers, G., Smith, B., Arneth, A., Jung, M., et al. (2015). The dominant role of semi-arid ecosystems in the trend and variability of the land CO_2 sink. *Science*, *348*(6237), 895–899. https://doi.org/10.1126/science.aaa1668

Ahmed, F., Rafii, M., Ismail, M. R., Juraimi, A. S., Rahim, H., Asfaliza, R., & Latif, M. A. (2013). *Waterlogging tolerance of crops: Breeding, mechanism of tolerance, molecular approaches, and future prospects*. BioMed research international.

Andrews, A. E., Kofler, J. D., Trudeau, M. E., Williams, J. C., Neff, D. H., Masarie, K. A., et al. (2014). CO_2, CO, and CH_4 measurements from tall towers in the NOAA Earth system research laboratory's global greenhouse gas reference network: Instrumentation, uncertainty analysis, and recommendations for future high-accuracy greenhouse gas monitoring efforts. *Atmospheric Measurement Techniques*, *7*(2), 647–687. https://doi.org/10.5194/amt-7-647-2014

Bloch, M., & Bhattacharjee, J. (2020). Characterizing the carbon fluxes of a bottomland hardwood forest. Paper presented at AGU Fall Meeting Abstracts 2020 (abstract #B065-0004).

Bourtsoukidis, E., Kawaletz, H., Radacki, D., Schütz, S., Hakola, H., Hellén, H., et al. (2014). Impact of flooding and drought conditions on the emission of volatile organic compounds of quercus robur and prunus serotina. *Trees*, *28*(1), 193–204. https://doi.org/10.1007/s00468-013-0942-5

Chevallier, F., Wang, T., Ciais, P., Maignan, F., Bocquet, M., Altaf Arain, M., et al. (2012). What Eddy-covariance measurements tell us about prior land flux errors in CO_2-flux inversion schemes. *Global Biogeochemical Cycles*, *26*(1). https://doi.org/10.1029/2010GB003974

Dalmagro, H. J., Zanella de Arruda, P. H., Vourlitis, G. L., Lathuillière, M. J., De, S., Nogueira, J., et al. (2019). Radiative forcing of methane fluxes offsets net carbon dioxide uptake for a tropical flooded forest. *Global Change Biology*, *25*(6), 1967–1981. https://doi.org/10.1111/gcb.14615

Davis, K. J., Browell, E. V., Feng, S., Lauvaux, T., Obland, M. D., Pal, S., et al. (2021). The atmospheric carbon and transport (ACT)-America mission. *Bulletin of the American Meteorological Society*, *102*(9), E1714–E1734. https://doi.org/10.1175/BAMS-D-20-0300.1

Davis, K. J., Deng, A., Lauvaux, T., Miles, N. L., Richardson, S. J., Sarmiento, D. P., et al. (2017). The Indianapolis Flux Experiment (INFLUX): A test-bed for developing urban greenhouse gas emission measurements. *Elementa: Science of the Anthropocene*, *5*, 5. https://doi.org/10.1525/elementa.188

Detmers, R. G., Hasekamp, O., Aben, I., Houweling, S., Van Leeuwen, T. T., Butz, A., et al. (2015). Anomalous carbon uptake in Australia as seen by GOSAT. *Geophysical Research Letters*, *42*(19), 8177–8184. https://doi.org/10.1002/2015GL065161

Dinsmore, K. J., Billett, M. F., & Dyson, K. E. (2013). Temperature and precipitation drive temporal variability in aquatic carbon and ghg concentrations and fluxes in a peatland catchment. *Global Change Biology*, *19*(7), 2133–2148. https://doi.org/10.1111/gcb.12209

Dlugokencky, E., & Tans, P. (2016). The marine boundary layer reference (downloaded early 2016). Retrieved from https://www.esrl.noaa.gov/gmd/ccgg/mbl/mbl.html

Dušek, J., Čížková, H., Czerný, R., Taufarová, K., Šmídová, M., & Janouš, D. (2009). Influence of summer flood on the net ecosystem exchange of CO_2 in a temperate sedge-grass marsh. *Agricultural and Forest Meteorology*, *149*(9), 1524–1530. https://doi.org/10.1016/j.agrformet.2009.04.007

Follett, R. (2001). Soil management concepts and carbon sequestration in cropland soils. *Soil and Tillage Research*, *61*(1), 77–92. https://doi.org/10.1016/S0167-1987(01)00180-5

Frank, D., Reichstein, M., Bahn, M., Thonicke, K., Frank, D., Mahecha, M. D., et al. (2015). Effects of climate extremes on the terrestrial carbon cycle: Concepts, processes and potential future impacts. *Global Change Biology*, *21*(8), 2861–2880. https://doi.org/10.1111/gcb.12916

Friend, A. D., Arneth, A., Kiang, N. Y., Lomas, M., Ogée, J., Rödenbeck, C., et al. (2007). Fluxnet and modelling the global carbon cycle. *Global Change Biology*, *13*(3), 610–633. https://doi.org/10.1111/j.1365-2486.2006.01223.x

Gelaro, R., McCarty, W., Suárez, M. J., Todling, R., Molod, A., Takacs, L., et al. (2017). The modern-era retrospective analysis for research and applications, version 2 (MERRA-2). *Journal of Climate*, *30*(14), 5419–5454. https://doi.org/10.1175/JCLI-D-16-0758.1

Guanter, L., Zhang, Y., Jung, M., Joiner, J., Voigt, M., Berry, J. A., et al. (2014). Global and time-resolved monitoring of crop photosynthesis with chlorophyll fluorescence. *Proceedings of the National Academy of Sciences*, *111*(14), E1327–E1333. https://doi.org/10.1073/pnas.1320008111

Haigh, T. R., Otkin, J. A., Woloszyn, M., Todey, D., & Felkley, C. (2022). Meeting the drought information needs of midwest perennial specialty crop producers. *Journal of Applied Meteorology and Climatology*, *61*(7), 839–855. https://doi.org/10.1175/JAMC-D-21-0105.1

Han, G., Chu, X., Xing, Q., Li, D., Yu, J., Luo, Y., et al. (2015). Effects of episodic flooding on the net ecosystem CO_2 exchange of a supratidal wetland in the yellow river delta. *Journal of Geophysical Research: Biogeosciences*, *120*(8), 1506–1520. https://doi.org/10.1002/2015JG002923

Heald, C. L., Jacob, D. J., Jones, D. B. A., Palmer, P. I., Logan, J. A., Streets, D. G., et al. (2004). Comparative inverse analysis of satellite (mopitt) and aircraft (trace-p) observations to estimate asian sources of carbon monoxide. *Journal of Geophysical Research*, *109*(D23). https://doi.org/10.1029/2004JD005185

Hilton, R. G., Galy, A., Hovius, N., Chen, M.-C., Horng, M.-J., & Chen, H. (2008). Tropical-cyclone-driven erosion of the terrestrial biosphere from mountains. *Nature Geoscience*, *1*(11), 759–762. https://doi.org/10.1038/ngeo333

Jiang, F., Ju, W., He, W., Wu, M., Wang, H., Wang, J., et al. (2022). A 10-year global monthly averaged terrestrial net ecosystem exchange dataset inferred from the ACOS GOSAT v9 XCO_2 retrievals (GCAS2021). *Earth System Science Data*, *14*(7), 3013–3037. https://doi.org/10.5194/essd-14-3013-2022

Knapp, A. K., Beier, C., Briske, D. D., Classen, A. T., Luo, Y., Reichstein, M., et al. (2008). 10 Consequences of more extreme precipitation regimes for terrestrial ecosystems. *BioScience*, *58*(9), 811–821. https://doi.org/10.1641/B580908

Koster, R. D., Darmenov, A. S., & Da Silva, A. M. (2015). The quick fire emissions dataset (QFED): Documentation of versions 2.1, 2.2 and 2.4 (Tech. Rep.).

Kramer, K., Vreugdenhil, S. J., & Van der Werf, D. (2008). Effects of flooding on the recruitment, damage and mortality of riparian tree species: A field and simulation study on the rhine floodplain. *Forest Ecology and Management*, *255*(11), 3893–3903. https://doi.org/10.1016/j.foreco.2008.03.044

Lal, R. (2019). Accelerated soil erosion as a source of atmospheric CO_2. *Soil and Tillage Research*, *188*, 35–40. https://doi.org/10.1016/j.still.2018.02.001

Los, S. O., Pollack, N. H., Parris, M. T., Collatz, G. J., Tucker, C. J., Sellers, P. J., et al. (2000). A global 9-yr biophysical land surface dataset from noaa avhrr data. *Journal of Hydrometeorology*, *1*(2), 183–199. https://doi.org/10.1175/1525-7541(2000)001<0183:agybls>2.0.co;2

Ma, X., Huete, A., Cleverly, J., Eamus, D., Chevallier, F., Joiner, J., et al. (2016). Drought rapidly diminishes the large net co2 uptake in 2011 over semi-arid Australia. *Scientific Reports*, *6*(1), 37747. https://doi.org/10.1038/srep37747

Masarie, K. A., Peters, W., Jacobson, A. R., & Tans, P. P. (2014). Obspack: A framework for the preparation, delivery, and attribution of atmospheric greenhouse gas measurements. *Earth System Science Data*, *6*(2), 375–384. https://doi.org/10.5194/essd-6-375-2014

Masarie, K. A., & Tans, P. P. (1995). Extension and integration of atmospheric carbon dioxide data into a globally consistent measurement record. *Journal of Geophysical Research*, *100*(D6), 11593–11610. https://doi.org/10.1029/95JD00859

Meena, R. S., Kumar, S., & Yadav, G. S. (2020). Soil carbon sequestration in crop production. In R. S. Meena (Ed.), *Nutrient dynamics for sustainable crop production* (pp. 1–39). Springer Singapore. https://doi.org/10.1007/978-981-13-8660-2_1

Miles, N., Richardson, S., Martins, D., Davis, K., Lauvaux, T., Haupt, B., & Miller, S. (2018). *Act-America: L2 in situ CO_2, CO, and CH_4 concentrations from towers, eastern USA*. ORNL DAAC.

Miyata, A., Leuning, R., Denmead, O. T., Kim, J., & Harazono, Y. (2000). Carbon dioxide and methane fluxes from an intermittently flooded paddy field. *Agricultural and Forest Meteorology*, *102*(4), 287–303. https://doi.org/10.1016/S0168-1923(00)00092-7

Molod, A., Takacs, L., Suarez, M., & Bacmeister, J. (2015). Development of the GEOS-5 atmospheric general circulation model: Evolution from MERRA to MERRA2. *Geoscientific Model Development*, *8*(5), 1339–1356. https://doi.org/10.5194/gmd-8-1339-2015

National Centers for Environmental Information. (2018). Assessing the U.S. Climate in September 2018. Retrieved from https://www.ncei.noaa.gov/news/national-climate-201809. Accessed 2 April 2023.

Neri, A., Villarini, G., & Napolitano, F. (2020). Intraseasonal predictability of the duration of flooding above national weather service flood warning levels across the U.S. midwest. *Hydrological Processes*, *34*(23), 4505–4511. https://doi.org/10.1002/hyp.13902

Oda, T., & Maksyutov, S. (2015). *ODIAC fossil fuel CO_2 emissions dataset (version name: ODIAC2016)*. Center for Global Environmental Research, National Institute for Environmental Studies. https://doi.org/10.17595/20170411.001

Oda, T., Maksyutov, S., & Andres, R. J. (2018). The open-source data inventory for anthropogenic co_2, version 2016 (odiac2016): A global monthly fossil fuel co_2 gridded emissions data product for tracer transport simulations and surface flux inversions. *Earth System Science Data*, *10*(1), 87–107. https://doi.org/10.5194/essd-10-87-2018

Ott, L. E., Pawson, S., Collatz, G. J., Gregg, W. W., Menemenlis, D., Brix, H., et al. (2015). Assessing the magnitude of CO_2 flux uncertainty in atmospheric CO_2 records using products from nasa's carbon monitoring flux pilot project. *Journal of Geophysical Research: Atmospheres*, *120*(2), 734–765. https://doi.org/10.1002/2014JD022411

Paustian, K., Six, J., Elliott, E., & Hunt, H. (2000). Management options for reducing CO_2 emissions from agricultural soils. *Biogeochemistry*, *48*(1), 147–163. https://doi.org/10.1023/a:1006271331703

Price, J. J., & Berkowitz, J. F. (2020). Wetland functional responses to prolonged inundation in the active Mississippi river floodplain. *Wetlands*, *40*(6), 1949–1956. https://doi.org/10.1007/s13157-020-01309-1

Randerson, J. T., Thompson, M. V., Malmstrom, C. M., Field, C. B., & Fung, I. Y. (1996). Substrate limitations for heterotrophs: Implications for models that estimate the seasonal cycle of atmospheric CO_2. *Global Biogeochemical Cycles*, *10*(4), 585–602. https://doi.org/10.1029/96GB01981

Reed, T., Mason, L. R., & Ekenga, C. C. (2020). Adapting to climate change in the upper Mississippi river basin: Exploring stakeholder perspectives on river system management and flood risk reduction. *Environmental Health Insights*, *14*, 1178630220984153. PMID: 33447043). https://doi.org/10.1177/1178630220984153

Reichle, R. H., Draper, C. S., Liu, Q., Girotto, M., Mahanama, S. P., Koster, R. D., & De Lannoy, G. J. (2017). Assessment of MERRA-2 land surface hydrology estimates. *Journal of Climate*, *30*(8), 2937–2960. https://doi.org/10.1175/jcli-d-16-0720.1

Reichle, R. H., Liu, Q., Koster, R. D., Draper, C. S., Mahanama, S. P., & Partyka, G. S. (2017). Land surface precipitation in MERRA-2. *Journal of Climate*, *30*(5), 1643–1664. https://doi.org/10.1175/jcli-d-16-0570.1

Reichstein, M., Bahn, M., Ciais, P., Frank, D., Mahecha, M. D., Seneviratne, S. I., et al. (2013). Climate extremes and the carbon cycle. *Nature*, *500*(7462), 287–295. https://doi.org/10.1038/nature12350

Rodgers, C. D. (2000). Inverse methods for atmospheric sounding: Theory and practice. *World scientific*, *2*.

Rosenzweig, C., Tubiello, F. N., Goldberg, R., Mills, E., & Bloomfield, J. (2002). Increased crop damage in the us from excess precipitation under climate change. *Global Environmental Change*, *12*(3), 197–202. https://doi.org/10.1016/S0959-3780(02)00008-0

Schuldt, K. N., Mund, M., Luijkx, I. T., Aalto, T., Abshire, J. B., Aikin, K., et al. (2021). Multi-laboratory compilation of atmospheric carbon dioxide data for the period 1957–2019, obspack_co2_1_GLOBALVIEWplus_v6. 1_2021-03-01, NOAA earth system research laboratory, global monitoring laboratory (dataset). *NOAA Earth System Research Laboratory, Global Monitoring Laboratory*, *10*, 20210801.

Schwalm, C. R., Williams, C. A., Schaefer, K., Baldocchi, D., Black, T. A., Goldstein, A. H., et al. (2012). Reduction in carbon uptake during turn of the century drought in western North America. *Nature Geoscience*, *5*(8), 551–556. https://doi.org/10.1038/ngeo1529

Stein, A. F., Draxler, R. R., Rolph, G. D., Stunder, B. J. B., Cohen, M. D., & Ngan, F. (2015). NOAA's HYSPLIT atmospheric transport and dispersion modeling system. *Bulletin of the American Meteorological Society*, *96*(12), 2059–2077. https://doi.org/10.1175/BAMS-D-14-00110.1

Sulla-Menashe, D., & Friedl, M. A. (2018). *User guide to collection 6 MODIS land cover (MCD12q1 and MCD12C1) product* (Vol. 1, p. 18). USGS.

Sun, B., Jiang, M., Han, G., Zhang, L., Zhou, J., Bian, C., et al. (2022). Experimental warming reduces ecosystem resistance and resilience to severe flooding in a wetland. *Science Advances*, *8*(4), eabl9526. https://doi.org/10.1126/sciadv.abl9526

Takahashi, T., Sutherland, S. C., Wanninkhof, R., Sweeney, C., Feely, R. A., Chipman, D. W., et al. (2009). Climatological mean and decadal change in surface ocean pCO_2, and net sea–air CO_2 flux over the global oceans. *Deep Sea Research Part II: Topical Studies in Oceanography*, *56*(8–10), 554–577. https://doi.org/10.1016/j.dsr2.2008.12.009

Turner, A. J., Köhler, P., Magney, T. S., Frankenberg, C., Fung, I., & Cohen, R. C. (2021). Extreme events driving year-to-year differences in gross primary productivity across the us. *Biogeosciences*, *18*(24), 6579–6588. https://doi.org/10.5194/bg-18-6579-2021

Van der Molen, M., Dolman, A., Ciais, P., Eglin, T., Gobron, N., Law, B., et al. (2011). Drought and ecosystem carbon cycling. *Agricultural and Forest Meteorology*, *151*(7), 765–773. https://doi.org/10.1016/j.agrformet.2011.01.018

Van der Werf, G. R., Randerson, J. T., Giglio, L., Collatz, G. J., Mu, M., Kasibhatla, P. S., et al. (2010). Global fire emissions and the contribution of deforestation, savanna, forest, agricultural, and peat fires (1997–2009). *Atmospheric Chemistry and Physics*, *10*(23), 11707–11735. https://doi.org/10.5194/acp-10-11707-2010

Wei, Y., Shrestha, R., Pal, S., Gerken, T., Feng, S., McNelis, J., et al. (2021). Atmospheric carbon and transport – America (ACT-America) data sets: Description, management, and delivery. *Earth and Space Science*, *8*(7), e2020EA001634. https://doi.org/10.1029/2020EA001634

Weir, B., Ott, L. E., Collatz, G. J., Kawa, S. R., Poulter, B., Chatterjee, A., & Pawson, S. (2021). Bias-correcting carbon fluxes derived from land-surface satellite data for retrospective and near-real-time assimilation systems. *Atmospheric Chemistry and Physics*, *21*(12), 9609–9628. https://doi.org/10.5194/acp-21-9609-2021

Yildirim, E., & Demir, I. (2022). Agricultural flood vulnerability assessment and risk quantification in Iowa. *Science of The Total Environment*, *826*, 154165. https://doi.org/10.1016/j.scitotenv.2022.154165

Yin, Y., Byrne, B., Liu, J., Wennberg, P. O., Davis, K. J., Magney, T., et al. (2020). Cropland carbon uptake delayed and reduced by 2019 midwest floods. *AGU Advances*, *1*(1), e2019AV000140. https://doi.org/10.1029/2019AV000140

Zaerr, J. B. (1983). 03) Short-term flooding and net photosynthesis in Seedlings of three Conifers. *Forest Science*, *29*(1), 71–78. https://doi.org/10.1093/forestscience/29.1.71

Zhang, W., & Villarini, G. (2021). Greenhouse gases drove the increasing trends in spring precipitation across the central USA. *Philosophical Transactions of the Royal Society A: Mathematical, Physical & Engineering Sciences*, *379*(2195), 20190553. https://doi.org/10.1098/rsta.2019.0553

Zhou, W., Chen, F., Meng, Y., Chandrasekaran, U., Luo, X., Yang, W., & Shu, K. (2020). Plant waterlogging/flooding stress responses: From seed germination to maturation. *Plant Physiology and Biochemistry*, *148*, 228–236. https://doi.org/10.1016/j.plaphy.2020.01.020

Zhou, Y., Williams, C. A., Lauvaux, T., Davis, K. J., Feng, S., Baker, I., et al. (2020). A multiyear gridded data ensemble of surface biogenic carbon fluxes for North America: Evaluation and analysis of results. *Journal of Geophysical Research: Biogeosciences*, *125*(2), e2019JG005314. https://doi.org/10.1029/2019JG005314

Zomer, R. J., Bossio, D. A., Sommer, R., & Verchot, L. V. (2017). Global sequestration potential of increased organic carbon in cropland soils. *Scientific Reports*, *7*(1), 1–8. https://doi.org/10.1038/s41598-017-15794-8

Zona, D., Lipson, D. A., Paw U, K. T., Oberbauer, S. F., Olivas, P., Gioli, B., & Oechel, W. C. (2012). Increased CO_2 loss from vegetated drained lake tundra ecosystems due to flooding. *Global Biogeochemical Cycles*. https://doi.org/10.1029/2011GB004037

Erratum

An affiliation has been added to coauthor Brad Wier since the original publication of this article: "Now at Morgan State University, Maryland, Baltimore, MD, USA." This may be considered the authoritative version of record.